Effect of Two-Way Air–Sea Coupling in High and Low Wind Speed Regimes

SUE CHEN,* TIM J. CAMPBELL,+ HAO JIN,* SAŠA GABERŠEK,# RICHARD M. HODUR,@ AND PAUL MARTIN+

* *Naval Research Laboratory, Monterey, California*
+ *Naval Research Laboratory, Stennis Space Center, Mississippi*
# *University Corporation for Atmospheric Research, Boulder, Colorado*
@ *SAIC, Monterey, California*

(Manuscript received 30 June 2009, in final form 12 November 2009)

ABSTRACT

A recent advance in the Coupled Ocean–Atmosphere Mesoscale Prediction System (COAMPS) is described and used to study two-way air–sea coupling and its impact on two different weather scenarios. The first case examines the impact of a hurricane-induced cold ocean wake on simulated changes in the structure of Hurricane Katrina. The second case investigates the effect of wind- and current-induced island wakes and their impact on the local electromagnetic (EM) and acoustic propagation characteristics in the Southern California Bight region. In the Katrina case, both the atmosphere and ocean show a strong response from air–sea interaction. The model results show that wind-induced turbulent mixing, vertical advection, and horizontal advection are the three primary causes of the development of the trailing cold ocean wake. A distinct spatial separation is seen in these three primary forcing terms that are generating the bulk of the cooling in the ocean mixed layer. An asymmetric tropical cyclone structure change has been documented in detail from a more realistic, full physics, and tightly coupled model. These changes include a broadening of the eye, a reduced radius of hurricane-force wind, and a pronounced inner-core dry slot on the west side of the storm. In the island wake experiment, many finescale variations in the wind, current, and static stability structure resulting from the two-way interaction are described. These variations take the form of narrow vorticity and temperature anomalies that are found to reside in the ocean and atmosphere well downwind from the Channel Islands. Upwind differences in the lower-atmospheric wind and thermal structure also arise and are found to have a small impact on the lee-flow structure and EM characteristics of the southernmost Channel Islands.

1. Introduction

The importance of air–sea interaction has been recognized since the early era of numerical prediction of the atmosphere and ocean. Air–sea interaction affects the prediction of many environmental features, such as tropical cyclones (TCs), land–sea-breeze circulation, cloud ceiling and visibility issues, and ocean currents. Tactical parameters that are derived from the model data, such as electromagnetic (EM) and acoustic propagation, are also sensitive to this kind of interaction. The coupling of state-of-the-art ocean and atmospheric models is essential to improving the forecasts of these and other phenomena because it allows for more accurate representation of the complicated physical processes that govern exchanges across the air–sea interface.

Researchers at the Naval Research Laboratory have been working on the Coupled Ocean–Atmosphere Mesoscale Prediction System (COAMPS)[1] for use in studying weather phenomena in the coastal zone since the mid-1990s. In the first renditions of this model described by Hodur (1997), the dynamical framework of both the atmosphere and ocean were cast using a similar set of governing equations. Subsequent testing determined, however, that using a separate dynamical framework for the ocean model produced better results, primarily because it allowed for a better treatment of steep ocean bathymetry (Hong et al. 2000). Improvements to the ocean model itself were examined by Martin (2000),

Corresponding author address: Sue Chen, Naval Research Laboratory, 7 Grace Hopper Ave., Stop 2, Monterey, CA 93943-5502. E-mail: sue.chen@nrlmry.navy.mil

[1] COAMPS is a registered trademark of the Naval Research Laboratory.

DOI: 10.1175/2009MWR3119.1

Report Documentation Page

Form Approved
OMB No. 0704-0188

1. REPORT DATE	2. REPORT TYPE	3. DATES COVERED
SEP 2010		**00-00-2010 to 00-00-2010**

4. TITLE AND SUBTITLE	5a. CONTRACT NUMBER
Effect of Two-Way Air-Sea Coupling in High and Low Wind Speed Regimes	5b. GRANT NUMBER
	5c. PROGRAM ELEMENT NUMBER
6. AUTHOR(S)	5d. PROJECT NUMBER
	5e. TASK NUMBER
	5f. WORK UNIT NUMBER
7. PERFORMING ORGANIZATION NAME(S) AND ADDRESS(ES) **Naval Research Laboratory,7 Grace Hopper Ave., Stop 2,Monterey,CA,93943-5502**	8. PERFORMING ORGANIZATION REPORT NUMBER
9. SPONSORING/MONITORING AGENCY NAME(S) AND ADDRESS(ES)	10. SPONSOR/MONITOR'S ACRONYM(S)
	11. SPONSOR/MONITOR'S REPORT NUMBER(S)

12. DISTRIBUTION/AVAILABILITY STATEMENT
Approved for public release; distribution unlimited

13. SUPPLEMENTARY NOTES

14. ABSTRACT

A recent advance in the Coupled Ocean?Atmosphere Mesoscale Prediction System (COAMPS) is described and used to study two-way air?sea coupling and its impact on two different weather scenarios. The first case examines the impact of a hurricane-induced cold ocean wake on simulated changes in the structure of Hurricane Katrina. The second case investigates the effect of wind- and current-induced island wakes and their impact on the local electromagnetic (EM) and acoustic propagation characteristics in the Southern California Bight region. In the Katrina case, both the atmosphere and ocean show a strong response from air? sea interaction. The model results show that wind-induced turbulent mixing, vertical advection, and horizontal advection are the three primary causes of the development of the trailing cold ocean wake. A distinct spatial separation is seen in these three primary forcing terms that are generating the bulk of the cooling in the ocean mixed layer. An asymmetric tropical cyclone structure change has been documented in detail from a more realistic, full physics, and tightly coupled model. These changes include a broadening of the eye a reduced radius of hurricane-force wind, and a pronounced inner-core dry slot on the west side of the storm. In the island wake experiment, many finescale variations in the wind, current, and static stability structure resulting from the two-way interaction are described. These variations take the form of narrow vorticity and temperature anomalies that are found to reside in the ocean and atmosphere well downwind from the Channel Islands. Upwind differences in the lower-atmospheric wind and thermal structure also arise and are found to have a small impact on the lee-flow structure and EM characteristics of the southernmost Channel Islands.

15. SUBJECT TERMS

16. SECURITY CLASSIFICATION OF:			17. LIMITATION OF ABSTRACT	18. NUMBER OF PAGES	19a. NAME OF RESPONSIBLE PERSON
a. REPORT **unclassified**	b. ABSTRACT **unclassified**	c. THIS PAGE **unclassified**	**Same as Report (SAR)**	**24**	

Standard Form 298 (Rev. 8-98)
Prescribed by ANSI Std Z39-18

who developed the Navy Coastal Ocean Model (NCOM). This ocean model is hydrostatic and can be run in standalone fashion, if desired, with the atmospheric model providing the necessary 2D atmospheric forcing at the upper boundary of the ocean model. When COAMPS and NCOM were initially run together, the coupling was exclusively one-way [i.e., with no sea surface temperature (SST) feedback to the atmospheric model] and was accomplished with the use of simple input/output (I/O)-based calls at predetermined times set at runtime.

Several validation studies over the Adriatic in the fall and winter of 2001 and the winter of 2003 showed that the tides, currents, temperature, and salinity simulated by the one-way coupling of COAMPS and NCOM compared well with observations (Pullen et al. 2003; Martin et al. 2006). The system was able to reproduce observed cyclonic and anticyclonic gyres during several bora wind events. The ocean prediction skill improved with higher-horizontal-resolution atmospheric forcing.

The sensitivity of air–sea interaction to high-wind weather events has also been observed by other investigators using different types of coupled systems. Over the deep ocean, high surface winds can force formation of cold water in the wake region of intense TCs. Using a coupling of the fifth-generation Pennsylvania State University–National Center for Atmospheric Research (PSU–NCAR) Mesoscale Model (MM5), the Princeton Ocean Model (POM), and the Wave Model (WAM), Bao et al. (2000) evaluated the development of Hurricane Opal and found the model-simulated hurricane intensity was sensitive to inclusion of sea-spray evaporation and less sensitive to the wave-age-dependent roughness length. Recently, a three-way, air–ocean–wave coupled system [i.e., the MM5 atmospheric model, the 3D Price–Weller–Pinkel (3DPWP) ocean model, and the Wave Watch III wave model] from the University of Miami (Chen et al. 2007) was used during the Coupled Boundary Layer Air–Sea Transfer (CBLAST)-Hurricane (Black et al. 2007) to provide field operation guidance.

One other major, two-way, air–ocean, coupled system used in operational forecasting applications is the Geophysical Fluid Dynamics Laboratory (GFDL) hurricane prediction system, which is coupled to the Princeton Ocean Model. It was found that the two-way coupling improved the hurricane central pressure forecast by 26% compared to the operational GFDL model at that time (Bender and Ginis 2000). Recent GFDL improvements include a better ocean model initialization (Bender et al. 2007).

Although coupled model studies have shown steady progress, coupled modeling remains a difficult task. Because the air–sea models within the coupled system are complex and the coupled system needs to run on massively parallel computer platforms for computational efficiency, researchers often keep the coupling mechanism as simple as possible to avoid the engineering difficulty of writing a message passing interface (MPI) code to couple these independent models together. As a result, these coupled systems usually lack flexibility and are not easily relocated to other geographical areas.

A memory-based and tightly coupled mesoscale modeling system that is numerically efficient and easily relocated to a region of interest would give researchers a useful tool for improving the understanding of air–ocean interaction. The goals of this paper are to present recent results from an effort to form such a coupled system using a new coupling technique based on the Earth System Modeling Framework (ESMF) and to evaluate the two-way coupled model results for two separate applications. COAMPS is the first limited-area model to adopt the ESMF technology for air–sea coupling. We first discuss the atmospheric and ocean models used for these studies in section 2. Section 3 contains the model grid setup and a comparison of the coupled and uncoupled results for two numerical experiments. Test case 1 is a 48-h simulation of Hurricane Katrina prior to landfall, and test case 2 is an early-winter prefrontal event over the southern coast of California. Section 4 is a summary of the coupled results. A description of the innovative, generalized, coupling method used in the ESMF regrid technology is provided in the appendix.

2. Descriptions of the coupled model

There are four primary components that compose the current ocean–atmosphere, two-way coupled system (Fig. 1). These include a nonhydrostatic atmospheric model, a hydrostatic ocean model, a coupler that handles the data exchange between each of the coupled components, and an ocean background field that provides SST fields where and when the area of the atmospheric grid exceeds that of the ocean-model domain. Work to include a wave component is ongoing and will be described in a future paper. Additional information on the ESMF technology and a generalized coupling method is described in the appendix.

a. Atmospheric model

The atmospheric model used in this study is the operational version of COAMPS that has been operational at the Fleet Numerical Meteorology and Oceanography Center (FNMOC) since 1996. The details of this nonhydrostatic modeling system can be found in Hodur (1997), while subsequent improvements to the model physics and MPI structure are described in Chen et al.

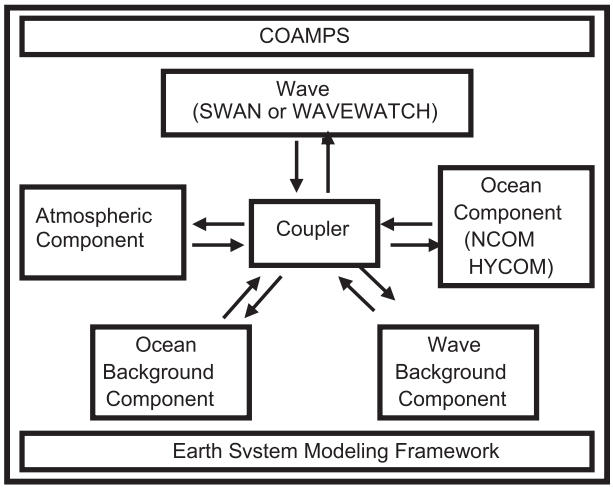

FIG. 1. A schematic plot of the COAMPS modeling framework. The coupling is achieved through the ESMF.

(2003). The SST feedback arises in this modeling system through a Monin–Obukhov-based, surface-similarity scheme. The surface fluxes are parameterized using standard bulk aerodynamic formulas:

$$\text{momentum flux: } U_*^2 = C_D \overline{U}^2, \tag{1}$$

$$\text{heat flux: } U_* \theta_* = C_H \overline{U}\,\overline{\Delta\theta}, \tag{2}$$

$$\text{moisture flux: } U_* q_* = C_E \overline{U}\,\overline{\Delta q}. \tag{3}$$

In these equations, U_* is the frictional velocity; θ_* is the scaling temperature; q_* is the vapor mixing ratio scaling; $\overline{U}$ is the mean surface wind speed; $\overline{\Delta\theta}$ and $\overline{\Delta q}$ are, respectively, the mean potential temperature and vapor mixing ratio differences as taken between the surface and the first model grid point above the surface; and C_D, C_H, and C_E are the transfer coefficients for momentum, heat, and moisture, respectively. The transfer coefficients are a function of the stability and roughness length as derived from observations. COAMPS uses the same roughness length for heat and moisture but a different roughness length for momentum. The stability function is a modified version of Louis (1979) based on version 3.0 of the Tropical Ocean and Global Atmosphere Coupled Ocean–Atmosphere Response Experiment (TOGA COARE; Fairall et al. 2003).

There is a large uncertainty in the magnitude of the heat, moisture, and momentum exchange coefficients under TC conditions because of a lack of observations. In COAMPS, the roughness length for momentum is modified to allow the momentum exchange coefficient to level off at wind speeds greater than 35 m s^{-1} (Jin et al. 2007), based on data from Donelan et al. (2004). The roughness lengths for heat and moisture are also modified (Dr. S. Wang 2009, personal communication) to account for the sea-spray effect that produces significant latent and sensible heat fluxes by droplet evaporation and thermal heat transfer (Andreas and Emanuel 2001; Bao et al. 2000). For neutral conditions over the ocean, the exchange coefficients can be represented by

$$C_{H,E} = \frac{1}{k} \ln \frac{z}{Z_{H,E}} \quad \text{and} \tag{4}$$

$$Z_{H,E} = \max(\text{COARE}, 3 \times 10^{-5} U_*^3), \tag{5}$$

where COARE is the COARE 3.0 bulk flux algorithm from Fairall et al. (2003); k is the Charnock parameter, which is a constant equal to 0.011; and $Z_{H,E}$ is the roughness length for heat and moisture.

b. Ocean model

The ocean component of the coupled system consists of the hydrostatic, mesoscale version of NCOM. NCOM employs a hybrid sigma–z-level vertical coordinate. At the ocean surface, the forcing fields from the atmospheric model are used as surface boundary conditions for momentum, potential temperature, and salinity as shown by Eqs. (6)–(9) (Martin 2000):

$$K_M \frac{\partial u}{\partial z} = \frac{\overline{\tau}_x}{\rho_0}, \tag{6}$$

$$K_M \frac{\partial v}{\partial z} = \frac{\overline{\tau}_y}{\rho_0}, \tag{7}$$

$$K_H \frac{\partial \theta}{\partial z} = \frac{\overline{Q}_b + \overline{Q}_e + \overline{Q}_s}{\rho_0 c_p}, \quad \text{and} \tag{8}$$

$$K_H \frac{\partial S}{\partial z} = S(\overline{E}_v - \overline{P}_r), \tag{9}$$

where K_M and K_H are vertical eddy coefficients for the momentum and scalar fields, respectively; u and v are the horizontal components of the current fields; θ and S are the potential temperature and salinity, respectively; τ_x and τ_y are the surface wind stress in the x and y directions, respectively; $\overline{Q}_b$, $\overline{Q}_e$, and $\overline{Q}_s$ are the net longwave, latent, and sensible surface heat fluxes, respectively; $\overline{E}_v$ and $\overline{P}_r$ are the surface evaporation and precipitation rates, respectively; and ρ_0 and c_p are the density and specific heat for seawater, respectively. The bars that appear on the right-hand side of Eqs. (6)–(9) indicate that these variables are time-averaged atmospheric quantities.

In one-way or two-way coupled mode, the atmospheric component provides a total of six fields to the

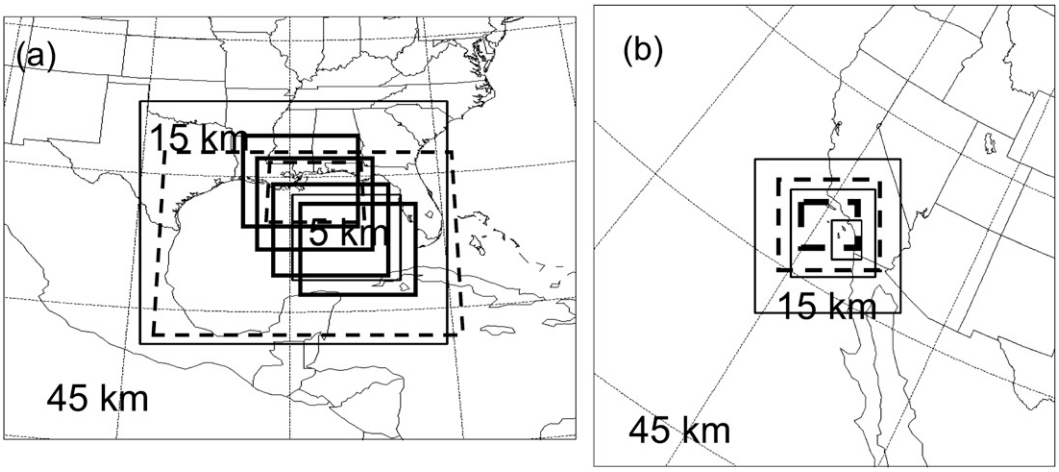

FIG. 2. The coupled model domain setup for the (a) Katrina and (b) Southern California test cases. The solid boxes depict the atmospheric-model domains and the dashed boxes depict the ocean-model domains. The Katrina 5-km atmospheric-model domain moves with the hurricane as depicted by the multiple box boundaries.

ocean component including the sea level pressure, the surface wind stress in the x and y directions in Eqs. (6) and (7), the total heat and moisture fluxes in Eqs. (8) and (9), and the net solar radiation. The net solar radiation is used to compute the diabatic heating contribution in the potential temperature equation (not shown). The sea level pressure is also needed as input for the pressure calculations in the momentum equations of the ocean model.

3. Results

We select Hurricane Katrina and an early winter prefrontal case with a predominantly northerly wind in the Southern California Bight to demonstrate the capability of the high-resolution, two-way coupled COAMPS.

a. Hurricane Katrina

After first making landfall along the southern Florida coast as a weak category 1 storm near 2230 UTC 25 August 2005, Katrina quickly strengthened to a category 5 storm by 1200 UTC 28 August as the storm entered the central Gulf of Mexico. Shortly after Katrina reached its maximum intensity, the storm weakened to a category 3 storm. This weakening appeared to correspond to the time the storm began to approach the shallow water of the Texas–Louisiana coastal shelf or approximately 18 h prior to making a second landfall near Buras, Louisiana, at approximately 1200 UTC 29 August. One striking feature associated with the period of weakening prior to the second landfall was the development of a 3–5-K cold SST anomaly evident in Katrina's wake (see Davis et al. 2008, their Fig. 8b). Such features have often been observed after the passage of typhoons and hurricanes and, once formed, may persist for many days after the passage of a given storm (Price et al. 2008).

The primary focus of this study is to investigate the air–sea interaction during the time of the wake development when Katrina weakened from a category 5 to a category 3 storm. To adequately capture this development, we begin the coupled model simulation at 1200 UTC 27 August 2005 and end the model run 48 h later at the time when Katrina was making its second landfall along the Louisiana coast. As shown in Fig. 2a, this experiment uses three atmospheric domains and two ocean domains. The outer two fixed atmospheric domains have horizontal grid resolutions of 45 and 15 km, while the innermost nest has a grid spacing of 5 km and automatically translates with the storm. The 5-km resolution is sufficient to capture most of the TC dynamic and thermodynamic processes but is too coarse to produce a detailed eyewall structure. Both ocean grids are fixed and have horizontal resolutions of 5 and 1.67 km. The atmospheric model has 60 vertical levels in which we vary the vertical grid spacing from 10 m near the surface to a maximum of 1000 m near the top. The ocean model is run with 40 vertical levels, including 19 terrain-following sigma layers in the upper 140 m and 21 fixed-depth levels between 140 m and the ocean bottom.

The atmospheric model was initialized using input from the global analysis derived from the GFS model. As is common with such procedures, the initial intensity error is large, though it quickly diminishes as the model spins up the circulation of the TC in response to the diabatic heating (Fig. 3). The initial TC intensity errors evident in Fig. 3 are on a par with similar studies (cf. Bender and Ginis 2000, their Fig. 5 at 1200 UTC 14 September and Davis et al. 2008, their Fig. 5b) and are

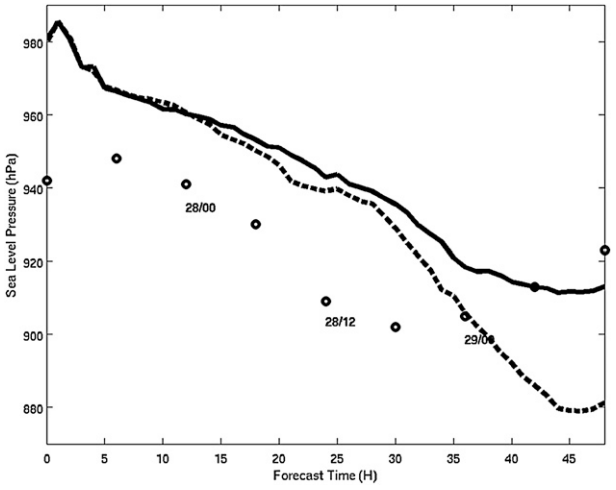

FIG. 3. Comparisons of minimum sea level pressure (hPa) derived using the observed and simulated conditions obtained from the atmospheric grid 3. The observed central pressures are plotted every 6 h (circles) beginning at 1200 UTC 27 Aug 2005. The dotted line denotes the pressure derived from the uncoupled run, while the solid line denotes the pressure values from the coupled run.

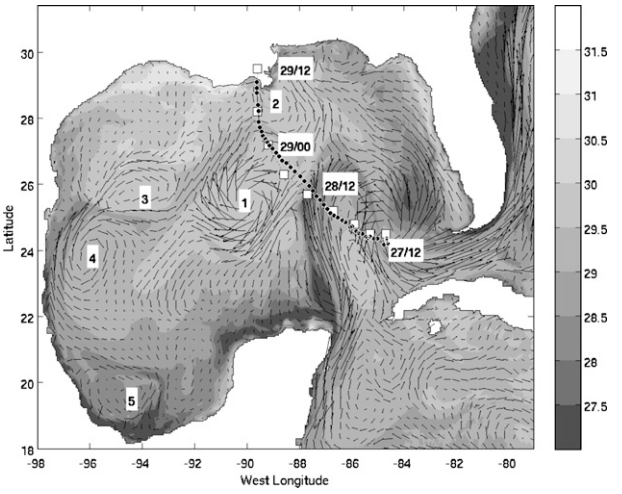

FIG. 4. Initial model SST (shaded) and surface current (vectors) for the Hurricane Katrina simulation from ocean grid 1. The numbers represent the locations of the cyclonic and anticyclonic rings (Gulf Loop Current eddies). The white squares depict the observed Katrina locations at 6-h intervals starting at 1200 UTC 27 Aug 2005, while the dotted line depicts the model-simulated Katrina locations at 1-h intervals for the 48-h simulation beginning at the same time. The maximum current vector is about 18 cm s^{-1}.

not unexpected given that Katrina was already very intense at the time of the start of the runs conducted here. Despite the large initial intensity error, the coupled model was able to spin up after 24 h and was close to the observed intensity 12 h prior to the second landfall. The model track, on the other hand, is quite good throughout the forecast (i.e., the model track lies slightly to the left of the observed best track by approximately 37 km throughout the forecast period).

To gauge the effect of including two-way coupled ocean–atmosphere modeling components on the simulated Katrina structure, we will compare the results to an uncoupled simulation that differs only in the specification of the SST field used throughout the 48-h simulation time. In both the coupled and uncoupled runs, the SST field is initially set to the SST valid at 1200 UTC 27 August (Fig. 4). The initial SST was obtained from NCOM by running a week of spinup in one-way mode using 3-hourly air–sea fluxes from the 0.2° FNMOC operational uncoupled COAMPS Central American run and lateral boundary condition from global NCOM. The primary difference in the way the uncoupled and coupled simulations were performed is that the SST field for the atmosphere in the uncoupled simulation remains fixed throughout the 48-h forecast, while we allow it to vary temporally and spatially in the coupled run. All the other aspects of the simulation, such as the initial conditions and lateral boundary conditions, are otherwise identical.

A comparison of the track obtained from the finest atmospheric mesh for the entire 48-h forecast shows that both forecasts have a very similar track when compared to the observed best-track estimate, which suggests that the overall movement of the simulated storm in this case is not overly sensitive to the coupling processes between the atmosphere and the ocean. The storm speed is very similar as well, with no significant difference in either simulated storm. Overall, we find that the simulated storms moved in good agreement with the observed storm, being somewhat faster during the first 30 h and

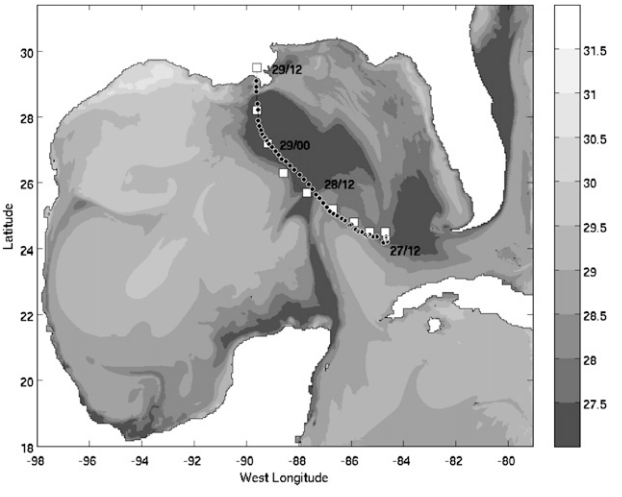

FIG. 5. Model-simulated SST (°C) at 48 h from ocean grid 1. The white squares denote the observed location of the eye at 6-h intervals and the dotted line denotes the model location of the eye at hourly intervals beginning at 1200 UTC 27 Aug 2005.

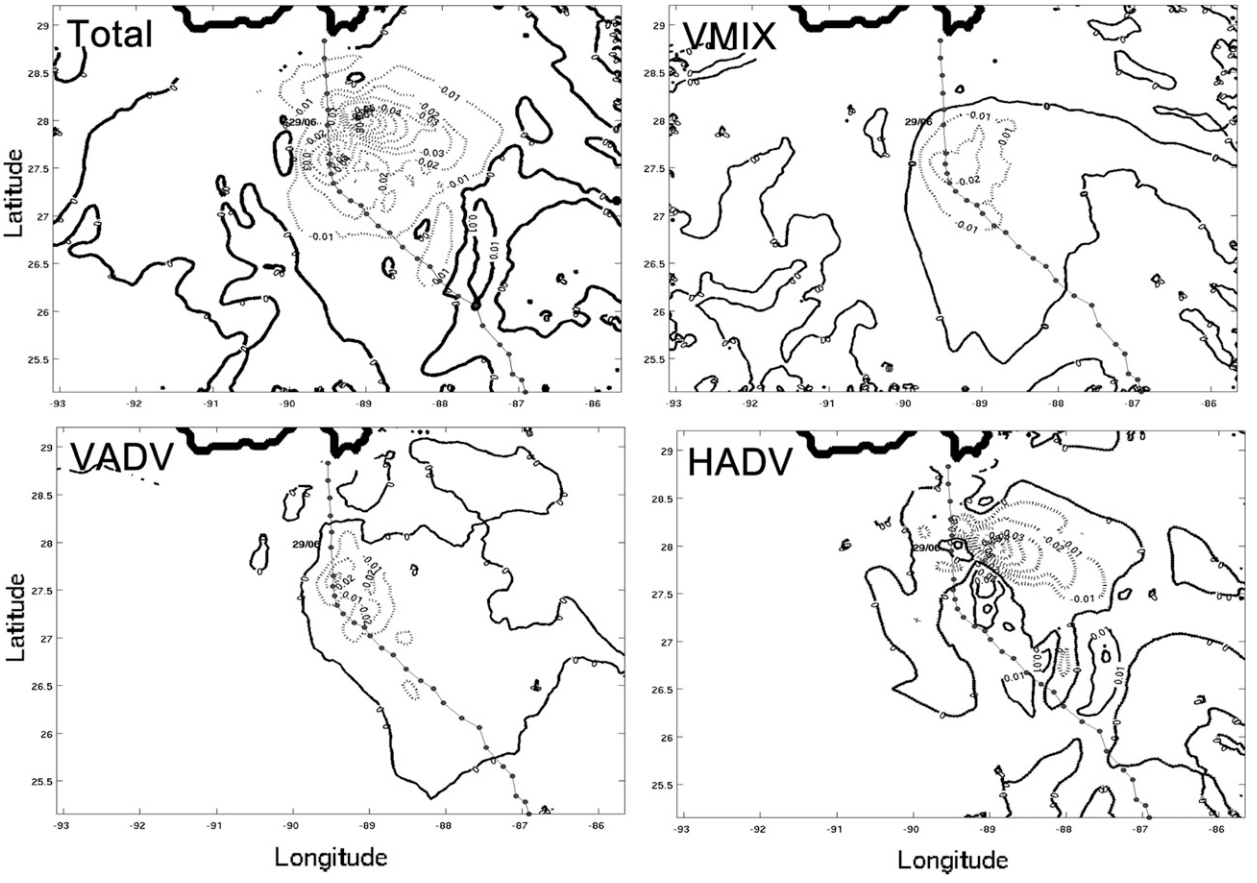

FIG. 6. Averaged mixed-layer ocean temperature change rate (°C h^{-1}) at 42 h. The total temperature change is the sum of the vertical mixing, vertical advection, and horizontal advection plus some smaller terms. The contour interval is 0.02°C h^{-1}.

somewhat slower after that point. The net effect was that both modeled storms made landfall within the simulated period of 48 h, suggesting that any changes in intensity were likely a result of model physics and ocean feedback processes rather than as a result of position errors.

Despite these similarities in the track and speed of the simulated storms, the storm intensity turned out to be quite different between the two cases. This has been noted to be the case in other coupled systems as well (Bender and Ginis 2000; Davis et al. 2008). Figure 3 shows the uncoupled simulation reached a much lower central pressure (i.e., 880 versus 915 hPa for the coupled run) with the trend in the uncoupled simulation to continue to intensify up until the storm made landfall. The coupled simulation, on the other hand, shows a reduction in the rate of deepening early in the forecast, with a much more pronounced reduction near 0000 UTC 29 August when the storm was still well offshore. It was also a time that corresponded well with the development of the TC cold wake. The structure and impact of this wake on the model dynamics are described in the following two sections.

1) UPPER-OCEAN RESPONSE TO THE COUPLING

The upper-ocean response to the strong surface wind forcing from the moving hurricane is the trailing asymmetric SST cooling and an enhanced current to the right of the storm track (Price 1981). Idealized ocean model studies by Price (1981) and Price et al. (1994), conducted with simplified bathymetry, suggested that the factors that affect the size and strength of the cold wake depend on the prestorm mixed-layer depth, the upper-ocean thermal stratification, the radius and strength of the maximum winds, the TC translation speed, and the local current inertial period. With these factors in mind, we now examine the characteristics of the TC cold wake and how it might differ from idealized studies when an inhomogeneous background current, asymmetric wind, real bathymetry, and two-way air–sea interaction are present.

The upper-ocean thermodynamic response to the imposed forcing derived from Katrina is shown in Figs. 5 and 6. Beginning with a plan view of the surface SST (Fig. 5), we find a well-defined cold wake approximately

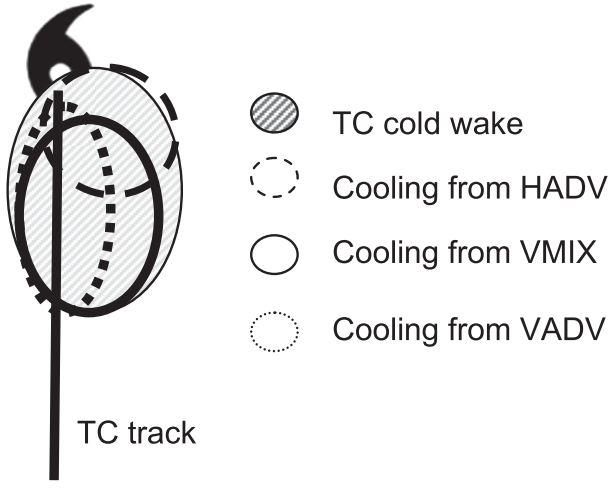

FIG. 7. A schematic plot of the wake cooling areas from horizontal advection, vertical mixing, and vertical advection.

150 km in width, preferentially created, as observed, to the right of the storm track. Overall, we find that the simulated width and length of this feature correspond well with the first available SST analyses obtained after the storm had cleared the Gulf (cf. Davis et al. 2008). The model-simulated lateral width of the cold wake is somewhat larger than in Davis et al. (2008) and the idealized study by Price (1981, see his Fig. 24). It is shown later in this section that this discrepancy may come from the contribution of cold water being advected by the mixed-layer currents, which is not considered in 1D mixed-layer ocean models such as the one used by Davis et al. (2008) and Price (1981).

When taken as an average over a 200 × 200 km^2 box centered on the area of greatest cooling at this time, the maximum depression of the SST is approximately 4.12°C, suggesting that a considerable alteration in the surface SST field occurs in response to the surface forcing of Katrina. Temporal and spatial fluctuations in the maximum cooling rate are found to arise within the cold wake, leading to local maximum temperature change of −7°C. Overall peak cooling rates of −0.3°C h^{-1} occur near 45 h (0900 UTC 29 August) when the storm intensity (measured by the model-simulated minimum SLP and maximum wind speed) starts to decrease (Fig. 3).

The physical processes that contribute to the spatial and temporal changes in the ocean temperature during the passage of Katrina are examined using an analysis of the upper-ocean temperature budget. In the NCOM

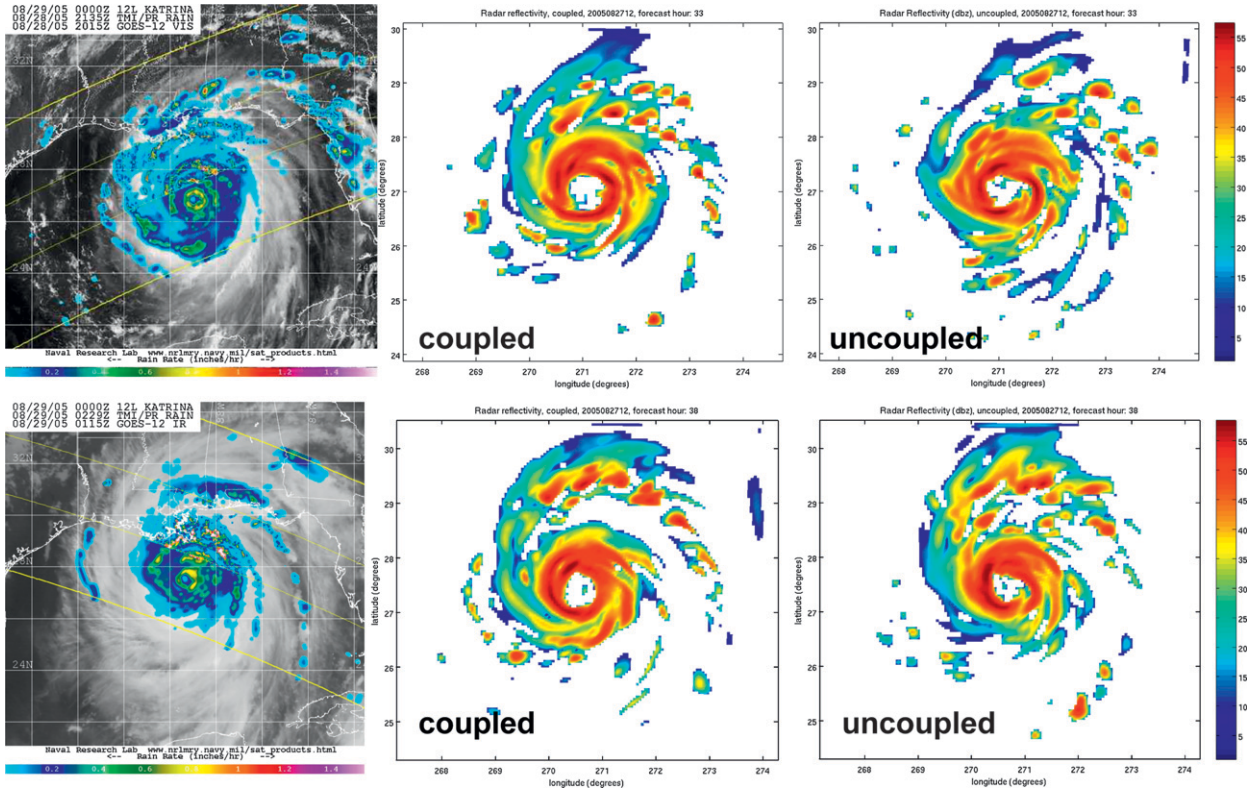

FIG. 8. TRMM estimated rain rate at (top left) 2135 UTC 28 Aug and (bottom left) 0229 UTC 29 Aug 2005. The model-simulated radar reflectivity (dBZ) at 2-km height from the (middle) coupled and (right) uncoupled runs shows a very similar structure, especially the heavy rainbands north of the eye. The radar reflectivity plots are taken at 2100 UTC 28 Aug and 0200 UTC 29 Aug 2005.

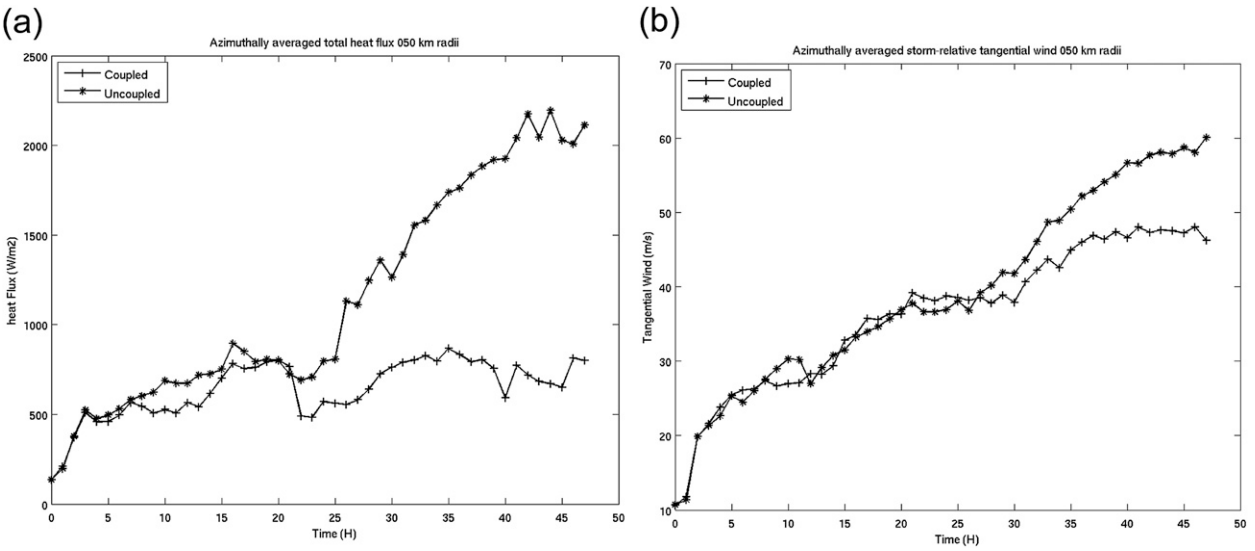

FIG. 9. The azimuthally averaged (a) total heat flux (W m^{-2}) and (b) maximum tangential wind (m s^{-1}). The averaging is done within a 50-km radius of the eye.

model, the rate of change of the SST is the sum of the changes due to horizontal advection and mixing, vertical advection (upwelling) and mixing, the surface heat flux, and solar radiation. The change due to horizontal mixing is small compared to the other terms and is therefore excluded from the budget analysis.

A plan view of the remaining ocean heat budget terms at 42 h is shown in Fig. 6. These fields represent an average over the depth of the mixed layer at a time when the storm was reaching peak intensity. A striking feature of the plot is the distinct spatial separation of the three primary forcing terms that are generating the bulk of the cooling. The total tendency reveals that two primary centers of cooling are occurring within the wake at this time, one centered along the storm track and the other displaced to the northeast in the storm's right-front quadrant. The northeastern center tends to be the stronger of the two and is found to be dominated by the horizontal advection term (Fig. 6d). The weaker cooling center, meanwhile, is nearly equally divided between contributions from the vertical mixing (Fig. 9b) and vertical advection terms (Fig. 9c) and is offset by warming associated with the horizontal advection term.

The results shown here illustrate that a variety of processes can contribute to the overall cooling of the wake. While these results stand somewhat in contrast to the TC wake cooling budget computed from the Hybrid Coordinate Ocean Model (HYCOM) simulations of Hurricane Ivan by Prasad and Hogan (2007, their Table 2 and Fig. 8), these differences may simply reflect the choice to present the data from individual model time or as an average field taken over the entire cold wake region. When averaged, the results from Prasad and Hogan (2007) suggest that the TC wake cooling is dominated by vertical mixing in the upper 20 m of the ocean and by vertical advection in the lower 50- and 100-m layers during the storm period. Our high-resolution results show that the processes contributing to the cooling can be quite different, depending on where the sampling is performed, as shown by our schematic illustration (Fig. 7). Within the mixed layer, the cooling from horizontal advection plays a larger role during the storm and post-maximum wind stress periods in our case. Below the mixed layer, our results agree with Price et al. (1994) and Prasad and Hogan (2007) that vertical advection is the main contributor to the storm period cooling. Our results also suggest that the cold-wake structure will not be fully represented by hurricane models coupled with a 1D mixed-layer model that does not have contributions from advection. The size of the wake in these models is, in general, smaller than in TC models coupled with a full-physics ocean circulation model. We will show in the next section that the width of the wake does have some impact on the TC flow structure in an idealized TC simulation.

2) ATMOSPHERE RESPONSE TO THE COUPLING

In this section, we describe the structural changes in the simulation of Hurricane Katrina that arise from the development of the cold wake. The results are displayed using azimuthally averaged fields taken about the storm center as well as azimuthally and time-averaged quadrant plots, which help elucidate asymmetrical aspects of the

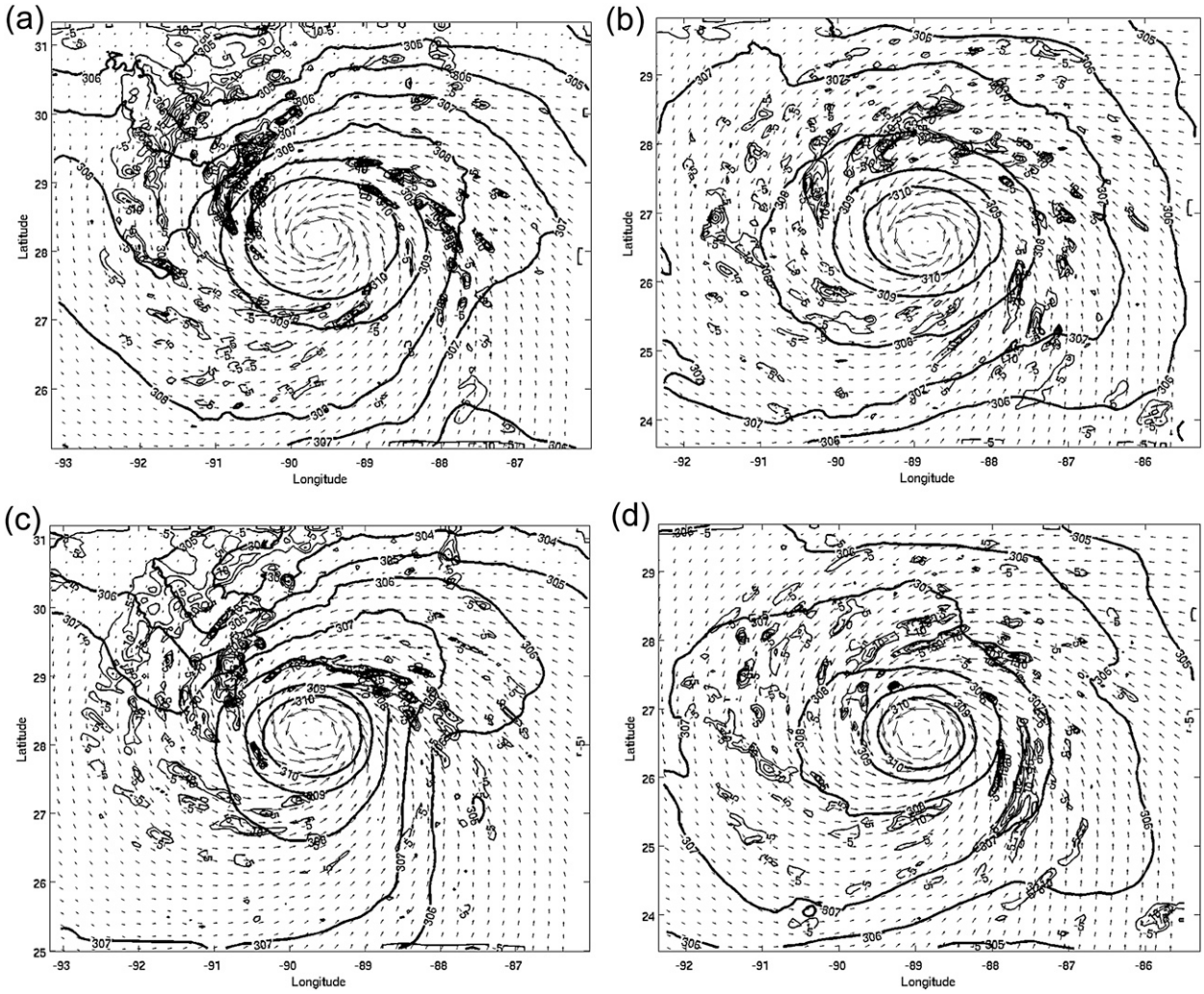

FIG. 10. Plan views of the 12-h mean 10-m wind vectors, divergence (s^{-1}), and virtual potential temperature (K) for the (a) coupled and (b) uncoupled runs between 20 and 32 h and the (c) coupled and (d) uncoupled runs between 33 and 45 h. Only the negative values of divergence are shown. The contour interval for the divergence is 1×10^{-6} s^{-1} and for the virtual potential temperature it is 0.5 K.

simulated storm structure. Several idealized axisymmetric vortex simulations are also conducted to aid the interpretation of the coupled model results.

A comparison of the model-derived reflectivity fields with available Tropical Rainfall Measuring Mission (TRMM) imagery shows good overall agreement of both the coupled and uncoupled model with the asymmetrical structure evident in the observed storm (Fig. 8). The plots are shown approximately 10 and 16 h after the coupled run began generating a cold wake in the SST field near 22 h. The impact of the wake is first seen in the azimuthally averaged latent heat flux, which is found to rapidly depart from the steadily increasing values obtained in the uncoupled run (Fig. 9). The structural changes in the low-level thermal fields and convergence patterns supporting the developing convection are shown in Fig. 10. The plots represent 12-hourly averaged fields taken just after the wake formed and 12 h later covering the period when the azimuthally averaged tangential wind in the uncoupled run began to surpass that of the coupled simulation. A striking feature of the temporally averaged fields is the changes in the low-level convergence and thermal fields that arise once the impact of the cold wake begins to take hold on the storm circulation. In particular, note the reduction in the low-level convergence centers over the southeast quadrant of the coupled run over the cold water (cf. Figs. 10a,c) and the development of the asymmetrical thermal field as a pronounced cold wedge forms on the eastern flank of the coupled storm (cf. Figs. 10c,d). While there is considerably more detail in the temporally averaged convergence fields in these simulations [as compared to

those obtained by Zhu et al. (2004)], we see a similar general counterclockwise shift in the band of the strongest convergence in the coupled run. In this case, the shift appears to be related to the reduction of the convergence over the cold wake and a corresponding increase in convergence over the northeast sector of the storm. This enhanced region of convergence resides where the low-level flow overruns the pronounced eastward-extending warm lobe that resides just to the north of the north–south-orientated cold wedge found over the southeast quadrant of the storm (Fig. 10c).

The increased flow asymmetry in the coupled run can be seen in the comparisons of the Hovmöller diagrams of the azimuthally averaged vertical velocity field at the 700-hPa level (Fig. 11a). It is evident that the eye in the uncoupled run is steadily contracting with time as the storm continues to intensify. In the coupled run, this tendency is interrupted as the maximum vertical velocity tends to remain at a fixed radial distance from the storm center. At the 400-hPa level, there is decreased vertical motion in the inner-core region in the southwest quadrant but a continuous deep vertical motion in the inner-core region in the wake and northeast quadrants (Fig. 12). Inspection of the Hovmöller diagrams of the tangential wind radius at 10-m height shows the maximum eye size for the coupled run is approximately 10 km larger than for the uncoupled run. However, the maximum azimuthally averaged hurricane-force wind speed (33 m s^{-1}) radius at 10-m height for the coupled run is approximately 9.3 km smaller than for the uncoupled run at 43 h (Fig. 11b). The results indicate about a 10% decrease of the TC circulation size due to the flow response to the cold wake. Thus, a broadening of the circulation occurs in the inner core but not in the outer regions of the storm.

Additional details of the structural differences in the simulated storms are shown through a series of azimuthally averaged fields displayed in each of the four storm quadrants (Figs. 13–16). The displayed fields include the height–radial plots of the equivalent potential temperature θ_e (Fig. 13), radial wind (Fig. 14), water vapor mixing ratio difference Q_v, equivalent potential temperature difference (Fig. 15), and vertical velocity (Fig. 16). To help reduce temporal fluctuations, the fields are displayed after taking a 3-h average between 42–45 h. Compared to the uncoupled run, the main thermodynamic differences in the coupled run include 1) lower θ_e and smaller upward motion in the inner-core region in all quadrants, 2) higher θ_e values in a broader secondary outflow in the lower and middle atmosphere in the southeast quadrants, 3) higher θ_e values in the southeast quadrants resulting from warmer temperature (not shown) and larger Q_v values, and 4) drier downdraft in the lower 3-km height of the inner-core region in the southwest quadrants.

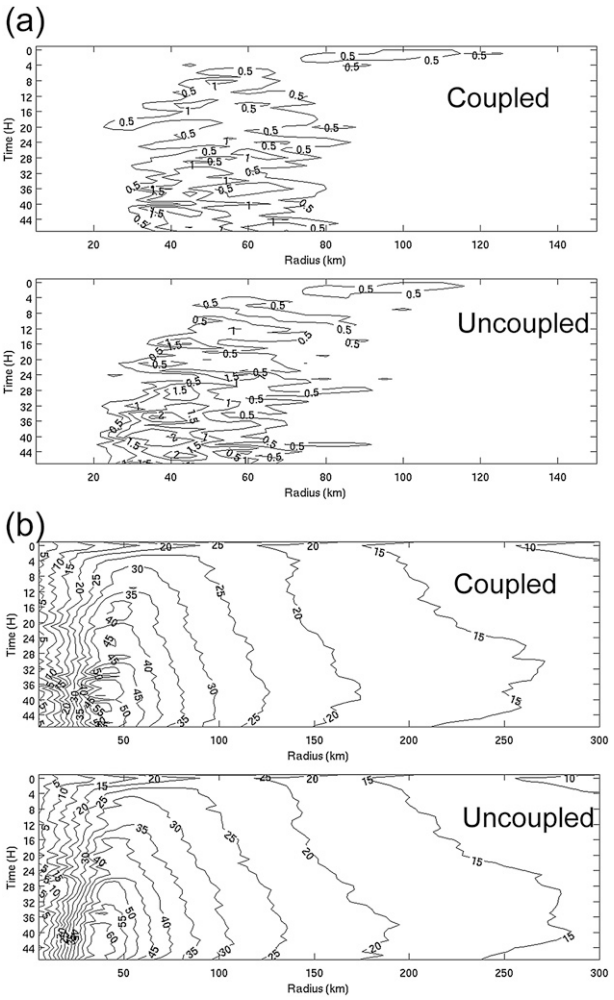

FIG. 11. Hovmöller diagram of azimuthally averaged (a) vertical velocity (m s^{-1}) at 700 hPa and (b) tangential wind (m s^{-1}) at 10 m. The contour interval is 0.5 m s^{-1} for the vertical velocity and 5 m s^{-1} for the tangential wind.

The lower θ_e and smaller upward motion in the inner-core region in all quadrants is due to the larger storm intensity in the uncoupled run. The broad region of warm and moist secondary outflow in the outer radius of the wake quadrant (Fig. 15) is related to the presence of the wider and shallower band of convection in the coupled run (Fig. 12). This feature is also seen in two recent Katrina rainband studies. Hence and Houze (2008) attributed the secondary outflow to the overturning rainband updrafts that occurred above the 3.5-km level. Results from Didlake and Houze (2009, see their Figs. 10 and 11) further indicated positive temperature perturbation in the rainband area in the southeast quadrant. Didlake and Houze (2009) related the warming in the 2–7-km levels to the overturning updrafts. Although our azimuthally and time-averaged cross-sectional analysis

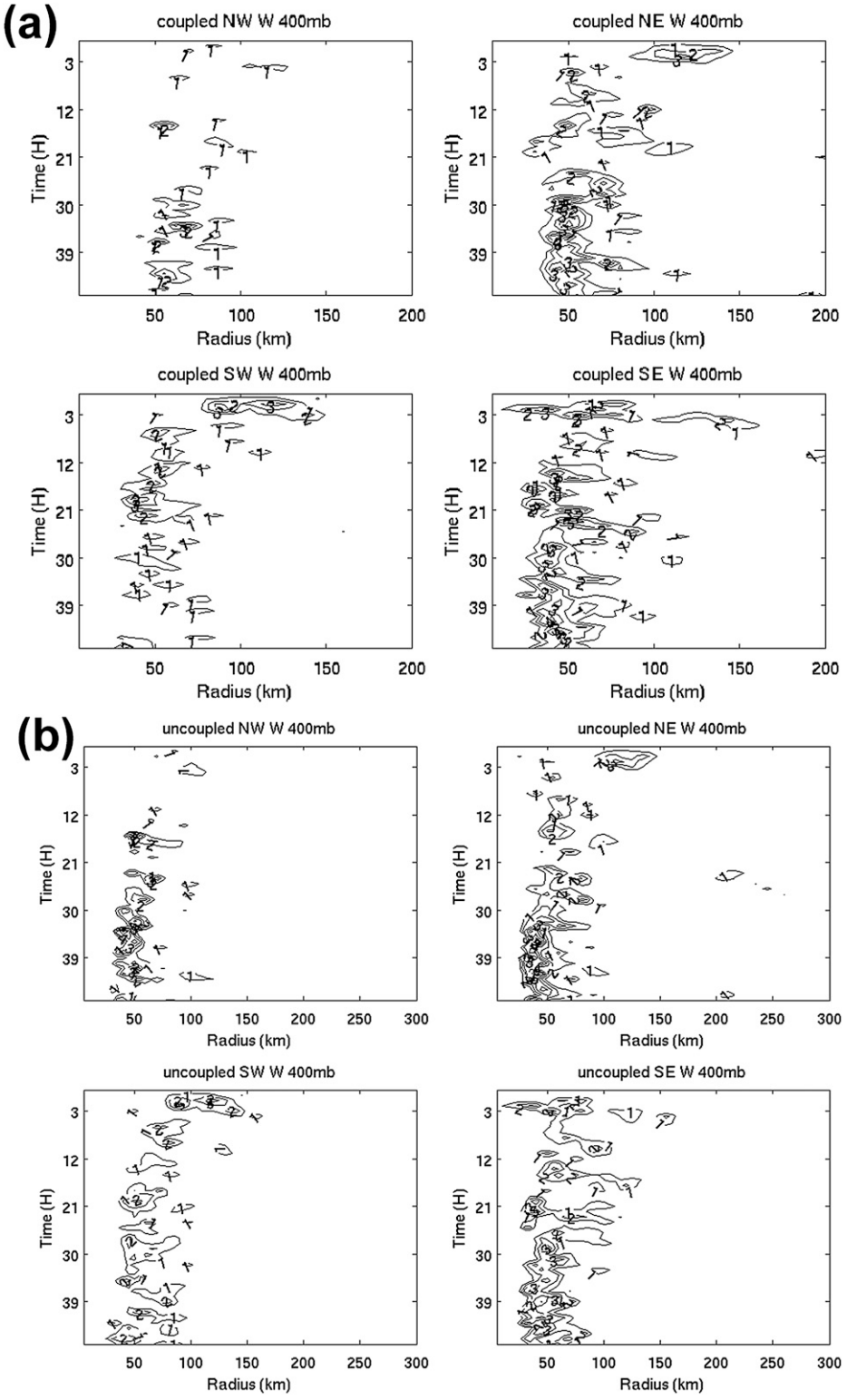

FIG. 12. Hovmöller diagram of azimuthally averaged vertical velocity (m s^{-1}) at 400 hPa for the (a) coupled and (b) uncoupled runs. The contour interval is 1 m s^{-1}.

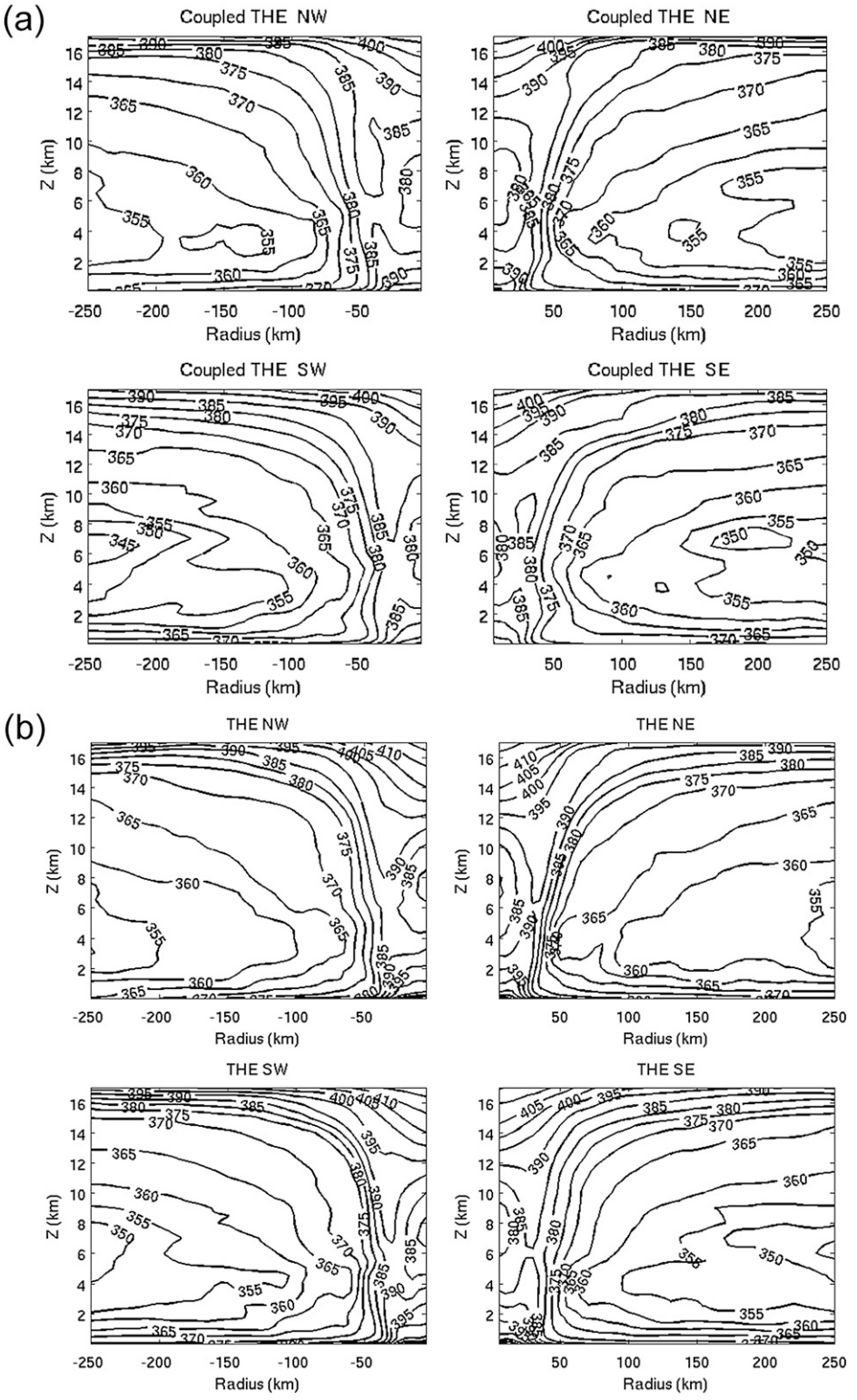

FIG. 13. Azimuthally and time-averaged equivalent potential temperature (K) for the (a) coupled and (b) uncoupled runs. The contour interval is 5 K.

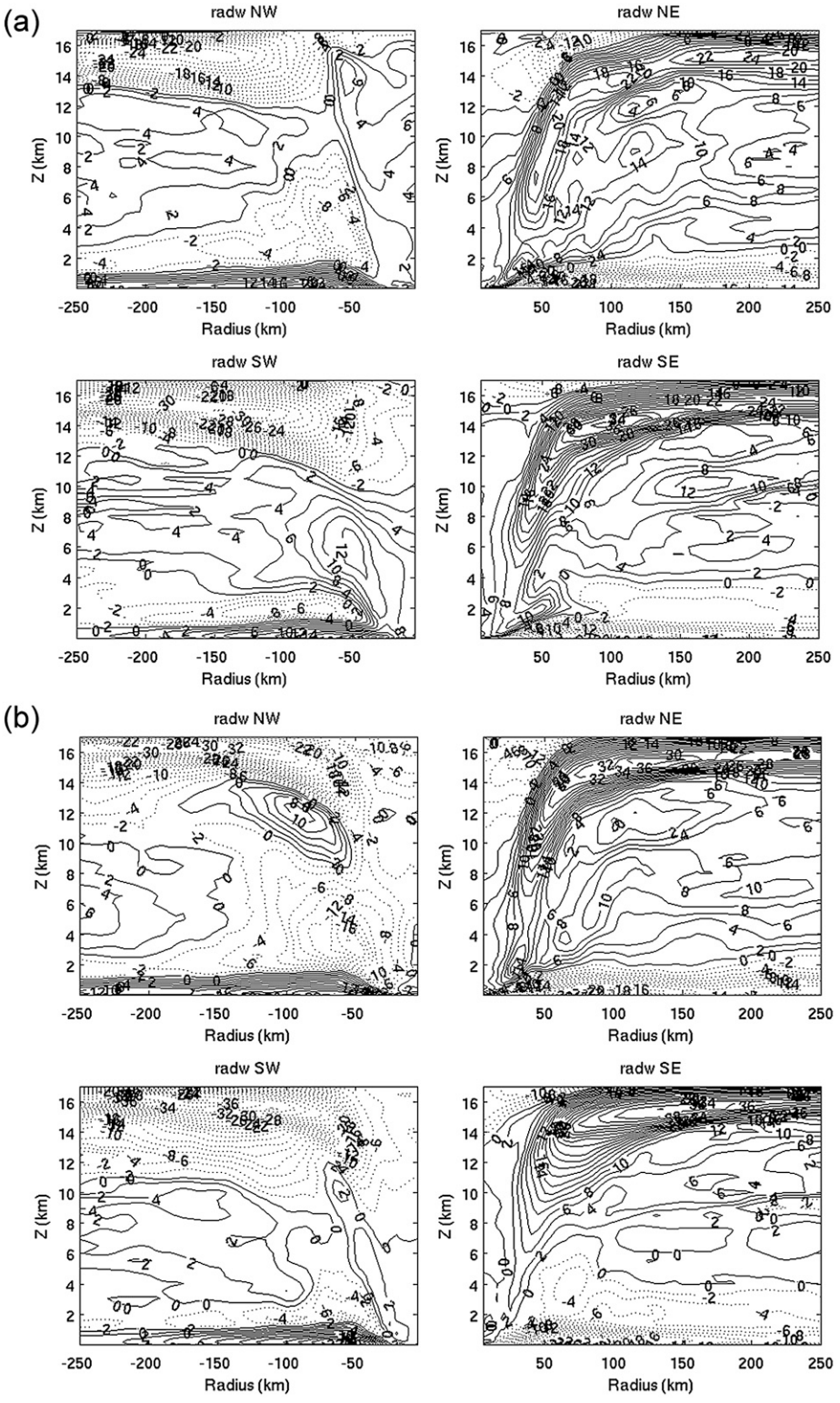

FIG. 14. Azimuthally and time-averaged radial wind (m s^{-1}) for the (a) coupled and (b) uncoupled runs. The contour interval is 2 m s^{-1}.

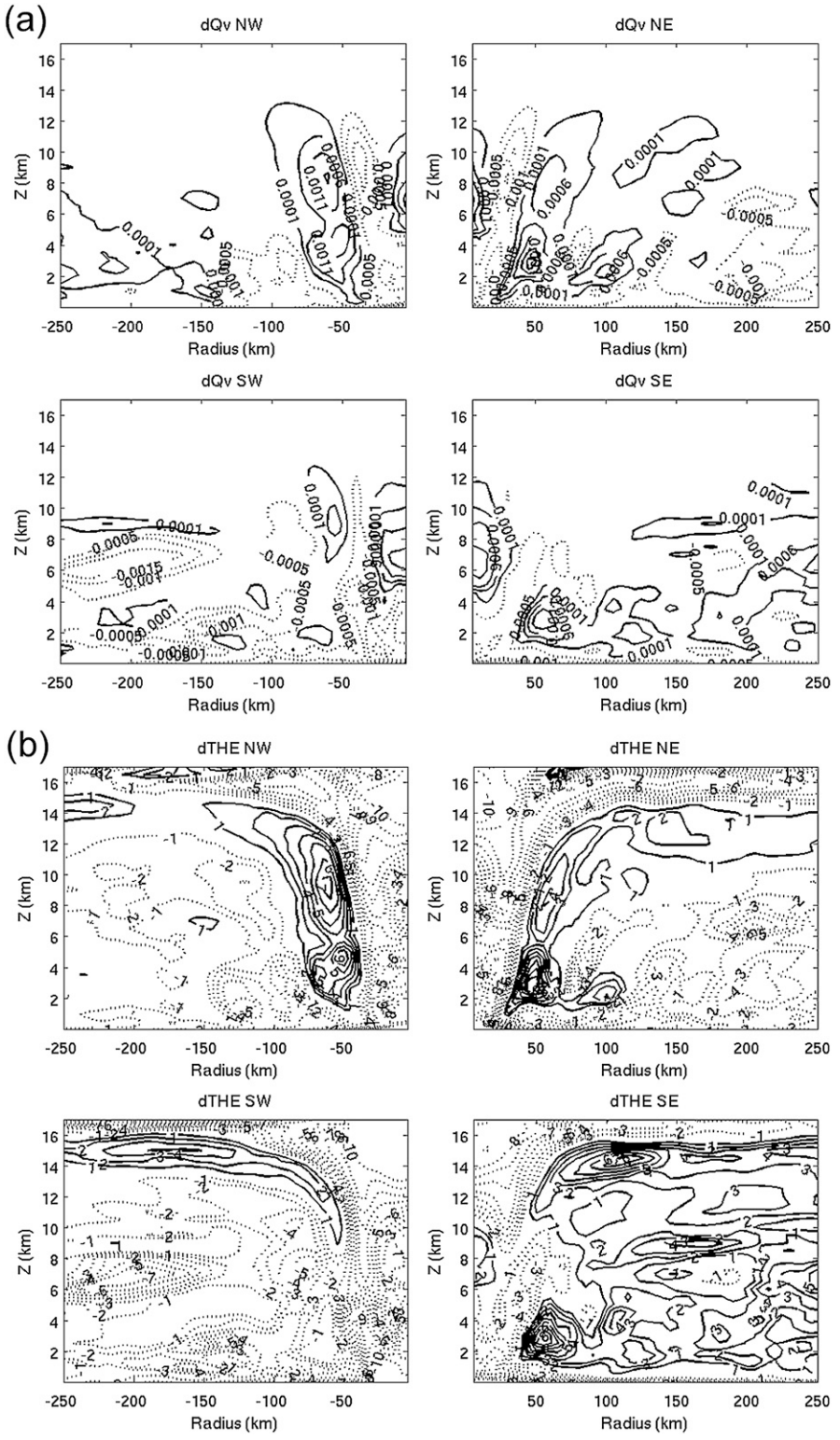

FIG. 15. Azimuthally and time-averaged coupled minus uncoupled differences for the (a) vapor mixing ratio (kg kg^{-1}) and (b) equivalent potential temperature (K). The contour interval for the vapor mixing ratio difference is 0.0005 kg kg^{-1}. The contour interval for the equivalent potential temperature difference is 1 K.

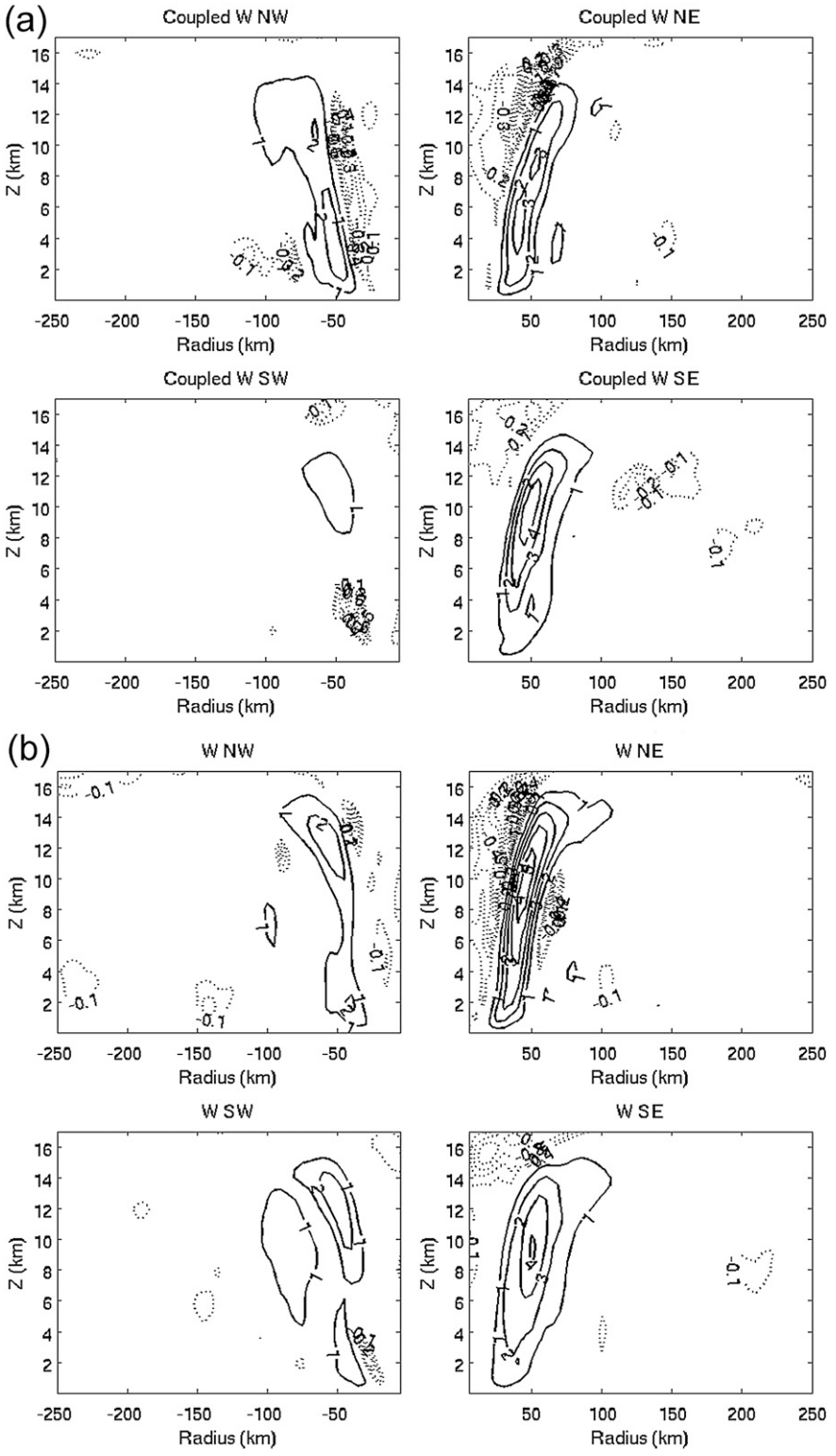

FIG. 16. Azimuthally and time-averaged vertical velocity (m s^{-1}) for the (a) coupled run and (b) uncoupled run. The contour interval for the positive values is 1 m s^{-1} and for the negative values is 0.1 m s^{-1}.

(0900 UTC 29 August) is 12 h later than the analysis time from these two studies, the general thermodynamic features obtained from our results over the southeast quadrant are consistent with theirs.

The dry slot seen in the downdraft area of the inner-core region on the west side of the model-simulated storm is remarkably similar to the observed lower fuselage radar image from WP-3D at 1028 UTC 29 August (Fig. 17). A strong principal rainband was observed east of the dry slot and there was a 700-hPa jet aligned with the rainband that was very unusual and may have been associated with the possible dry intrusion and the opening of the eye wall prior to and during landfall (Dr. P. Black 2009, personal communication). This rainband structure is also simulated in the coupled model (not shown), suggesting the wake may have played a role in the thermodynamic change that formed the dry slot.

The TC wind response to the onset of the cold wake has some similarity to the wind and SST front coupling studies reviewed by Small et al. (2008). To study how a laterally sheared flow over the wake might differ from the idealized SST fronts study by Spall (2007), we now consider the response of an axisymmetric flow over an imposed SST front that takes the form of a rectangular-shaped temperature anomaly. We set a constant temperature anomaly of -4 K over an otherwise uniform SST field with the width of the box set to 100 km. The initial wind field is specified as a Rankine vortex. All the idealized runs have the convection turned off, and the horizontal grid resolution of these dry simulations is 10 km. The response of the model flow fields is then studied by comparing the simulation with and without the temperature anomaly. In the third idealized run, the width of the cold anomaly is further reduced to 50 km to investigate the sensitivity of the mean flow change to the horizontal scale of the wake.

Compared with the results from Spall (2007), the low-level wind response is quite different in our case because of the strong rotation about the storm center. An interesting aspect of the simulations with the wake is that this run develops a significant horizontal wind asymmetry after 7 h of simulation. This pattern is perhaps best seen in the low-level vertical velocity pattern that arises as the flow adjusts to the imposed SST anomaly (Fig. 18b). Note that the overall structure that emerges is that of a wavenumber 3 pattern, consisting of three updraft–downdraft couplets in the vertical velocity field. These three updraft centers are located in the right-front, right-rear (over the wake), and left-front quadrants. In contrast, the flow from the run without the wake remains symmetric (Fig. 18a). In a run with a reduced wake size (50 km), there is also a wavenumber 3 response, but the horizontal flow response and the

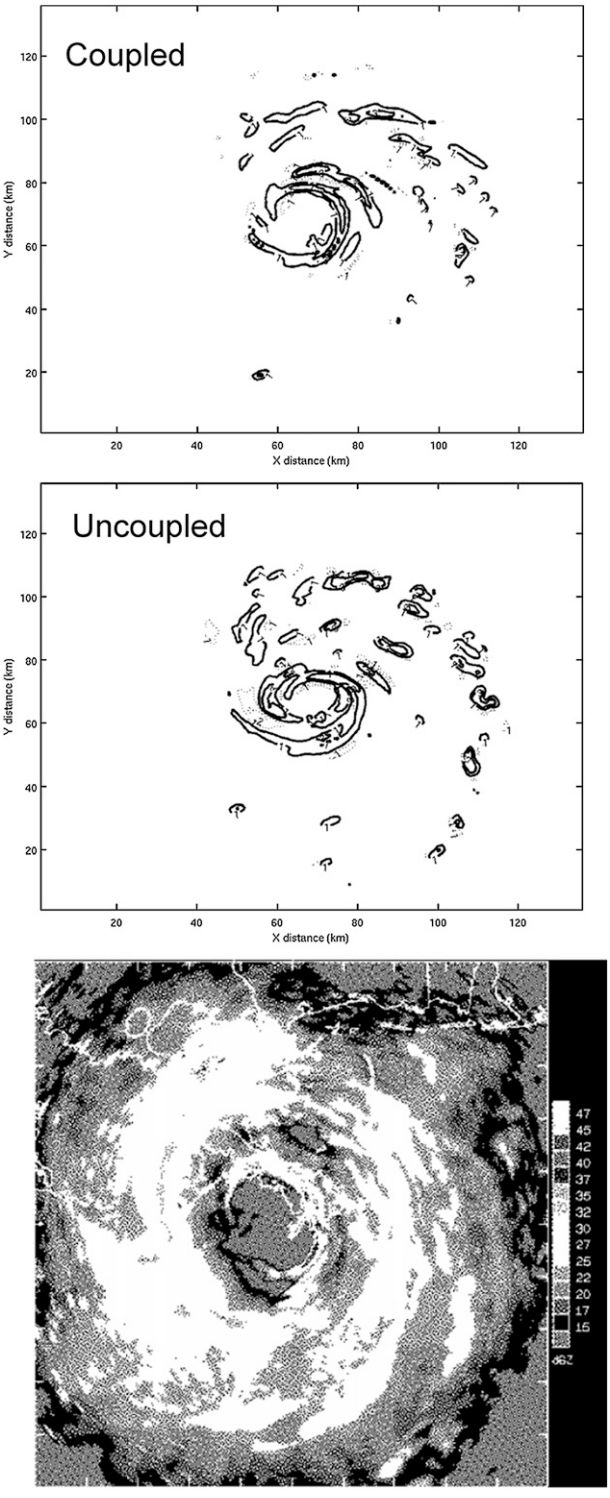

FIG. 17. Plan views of the model-simulated 700-hPa vertical velocity (m s^{-1}) at 0900 UTC 29 Aug 2005 from the (top) coupled and (middle) uncoupled runs. (bottom) An opening in the eyewall is seen in the lower fuselage radar image from WP-3D at 1028 UTC 29 Aug 2005.

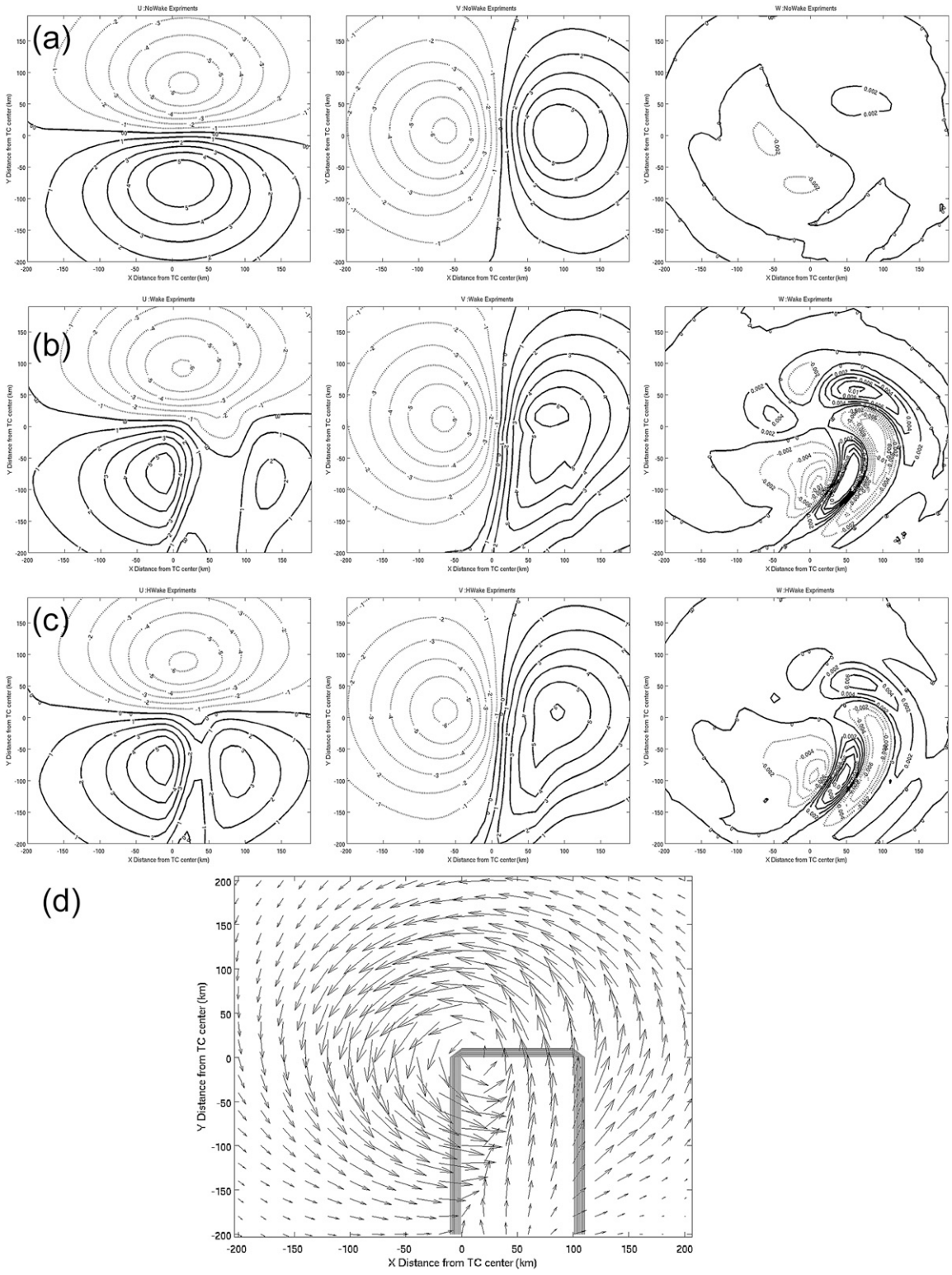

FIG. 18. (a) Idealized 24-h uncoupled dry hurricane simulations with uniform SST (300 K). The u and v at 10 m and w at 2.5 km are shown. The u and v contour interval is 1 m s^{-1} and the w contour interval is 0.001 m s^{-1}. (b) As in (a), but with a uniform 4-K, 100-km-wide cold wake. (c) As in (b), but the wake width is reduced to 50 km. (d) Wind field at 10 m for (b). The area of the cold wake is depicted by the thick lines.

updraft and downdraft magnitudes are smaller than in the 100-km-wide wake case (Fig. 18c).

The formation of these couplets can be understood by extending the analysis of Spall (2007). He suggested that the change in wind speed and direction across an idealized SST front in conditions of high-wind speed is to balance the Coriolis force due to the sudden change in turbulent mixing and boundary layer height of the flow as it crosses the SST front. The pressure gradient term in the momentum equation for this condition is neglected because the adjustment time scale is much smaller than the time scale in which the pressure gradient can act on the flow. The zonal and meridional wind forced by the SST front sets up surface convergence and divergence regions downwind from the front, which in turn induce a secondary circulation above the boundary layer due to a thermowind balance. He showed that winds blowing from warm to cold water tend to slow down and accelerate toward the lower background pressure gradient along the SST front, while winds blowing from cold to warm water accelerate the along-SST-front flow toward the higher background pressure gradient. As in the Spall study, parcels passing over the colder water decelerate and turn to the left toward lower pressure. As the parcels exit the cold wake a subsequent reacceleration and an outward turning are evident (Fig. 18d). Inertial effects then lead to an oscillating pattern in the flow field as the parcels continue to spin about the vortex. An interesting feature in the idealized runs with the wake is the development of a downward vertical motion upwind from the wake at the 2.5-km level in the southwest quadrant. This pattern has some similarity to the asymmetric Katrina coupled run where a downward vertical motion is also produced in the inner core in the southwest quadrant. Additional studies are planned to determine whether a similar mechanism is acting on the asymmetry evident in the full-physics coupled run.

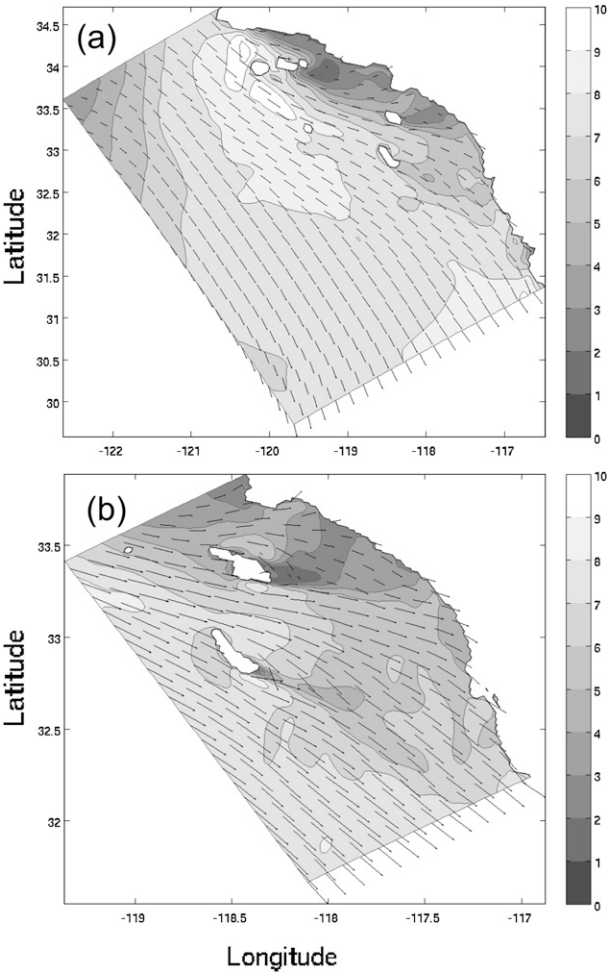

FIG. 19. Model-simulated 10-m wind speed (m s^{-1}, shaded contour) and wind direction (vectors) from the atmospheric (a) grid 3 and (b) grid 4. The maximum wind vector is approximately 10 m s^{-1}.

b. Eastern Pacific case

As a second application of the newly developed, coupled COAMPS system, we examine the problem of determining tactical weather parameters such as EM and sound propagation in a region of complex orography and bathymetry. Previous studies have shown that the complex flow around complex terrain leads to rapid local-scale variations in the conditions that support EM wave trapping. A study of steady flow past an isolated island by Burk et al. (2003), for example, attributed local variability in the trapping EM conditions to changes in the vertical structure of the vapor and temperature fields due to low-level blocking of the ambient flow and vortex shedding in the lee of the island. Our interest is to revisit this type of problem with the exception that we now allow a full ocean–atmospheric exchange to modify the conditions that arise in the lee of a given number of offshore islands to determine if the wake structure established in the ocean currents can significantly modify the lee EM structure in the atmosphere.

For this initial study, we have chosen to model the current and atmospheric flow over the Southern California Bight region. This region is influenced not only by the mountains along the irregularly shaped coastline, but also by the number of small islands (the eight so-called Channel Islands) of varying heights and dimensions found just offshore of the Southern California coast (Fig. 19). Because of the small scale of the Channel Islands, the model domains for the atmospheric and ocean models both consist of an inner grid with a grid spacing of 1.67 km. The 1.67-km atmospheric innermost nest covers the two southernmost islands, Santa Catalina

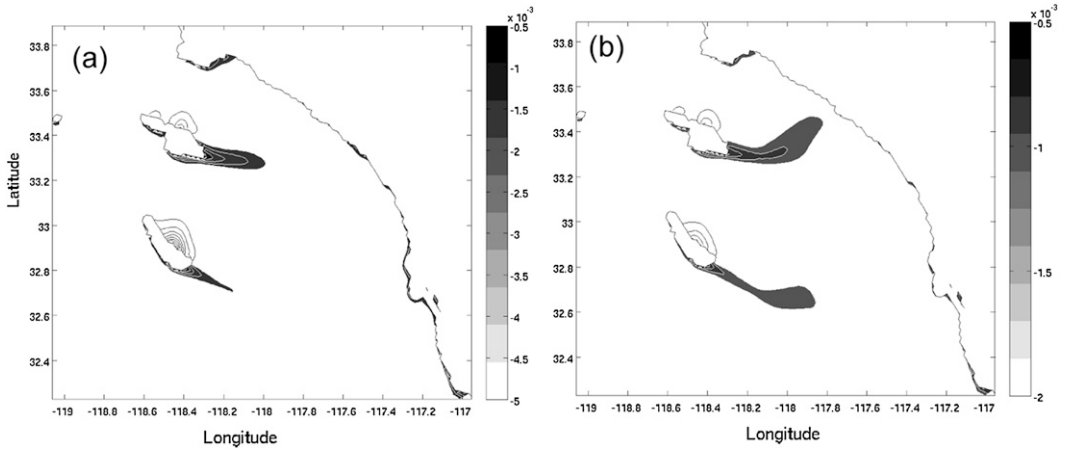

FIG. 20. Relative vorticity (s^{-1}) at 10-m height from the (a) coupled and (b) uncoupled runs from atmospheric grid 4. The contour interval is 0.006 s^{-1}.

and San Clemente, while the 1.67-km innermost ocean nest includes all but Anacapa and Santa Barbara Islands, which are too small to be well resolved at this grid spacing. The islands of Santa Catalina and San Clemente are effectively north–south-oriented, long, narrow islands. San Clemente is approximately 39 km long and 18 km wide, while Santa Catalina is approximately 35 km long and 13 km in maximum width. Both islands have small mountains that have peak elevations of approximately 600 m above sea level. In addition to the 1.67-km nests, the coupled model has three outer atmospheric domains and one ocean domain as shown in Fig. 2b. Both the atmospheric and ocean grids are set up using a Lambert Conformal Projection. The number of vertical levels for the atmospheric model is 30 and for the ocean model is 36, with 24 sigma layers and 12 fixed-depth levels. The initial and lateral boundary conditions are obtained from the Navy Operational Global Atmospheric Prediction System (NOGAPS) and global NCOM. The two-way air–sea interaction and its influence on the island wake effect and the EM and acoustic propagation in the wake region is compared with an uncoupled atmospheric simulation.

To assess the ability of the coupled model to produce small-scale fluctuations in the tactical weather parameters, we examine the model fields for a fixed period of time taken at the end of a 24-h simulation that was initialized at 0000 UTC 1 November 2006. As is typical of this region, the flow just offshore shows a complex structure due largely to its interaction with the coastal terrain. The primary feature of interest in this case is the location of the strong speed maxima in the northerly flow that extends downwind from Pt. Conception (Fig. 19a). Several of the Channel Islands, including San Clemente, are located within this belt of stronger winds. Relatively weaker flows closer to shore, as the air parcels traverse through the Channel Islands, show a tendency to turn toward the California coast.

The precise location of the shear zone between Catalina and San Clemente Islands becomes clearer when viewed on the finest atmospheric grid (Fig. 19b). It becomes evident from this figure that a much stronger ambient wind is found upstream from San Clemente than over Santa Catalina, even though the two islands are separated by less than 20 km. The response to this difference is evident in the lee of both islands, both in terms of the atmospheric relative vorticity and the surface wind stress.

A comparison of the vorticity structure of the coupled and uncoupled runs obtained on grid 4 of the atmospheric model shows subtle differences in the windward and wake regions of both the San Clemente and Catalina Islands (Fig. 20). In general, the wake structure of the uncoupled run extends much farther downstream from each island and each wake is seen to consist of higher relative vorticity values than are found in the coupled run. Plots of the difference in the low-level wind speed between the two runs (Fig. 21) indicate a maximum speed difference of less than a meter per second between the two runs. A consistent finding was that the upwind flow in the uncoupled run was slightly weaker and the static stability slightly higher due to differences in the SSTs. Both factors would contribute to slight differences in the local Froude number just upwind of the barriers in the uncoupled run, which possibly account for some of the simulated differences in the downstream flow structure. Thus, it may be important in some situations to account for changes in the upwind thermodynamic structure derived from a fully coupled run when considering the impact on the lee-flow structure.

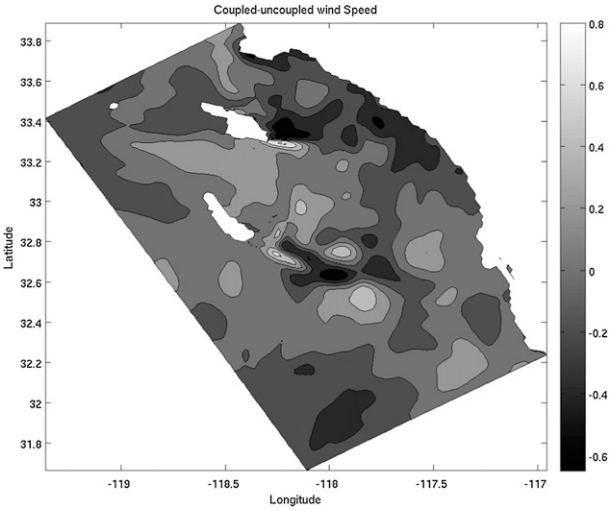

FIG. 21. The 10-m wind speed difference (m s^{-1}) at 24 h between the coupled and uncoupled runs from atmospheric grid 4.

1) OCEAN CIRCULATION STRUCTURE

The structure of the ocean circulation obtained in our coupled simulation is shown in Fig. 22. One of the striking features evident is the presence of the narrow vorticity streamers in the wake of all eight Channel Islands similar to the current wakes described by DiGiacomo and Holt (2001), Caldeira et al. (2005), and Dong and McWilliams (2007). In each case the vorticity banners extend downstream several times the length of any given island. It can be seen that the current wakes from San Miguel, Santa Rosa, and Santa Cruz reach San Nicolas and create a complex current structure upwind of San Nicolas, leading to a complex wake structure evident over 100 km downwind from this particular island.

2) EM AND SOUND PROPAGATION VARIABILITY DUE TO LEE WAKE STRUCTURE

Considerable variability in the atmospheric and ocean circulations arises in the wake of the Channel Islands due to the many fine-scale variations in the upstream wind, current, and static stability in the Southern California Bight region. The reduction of moisture with altitude creates an EM ducting condition, while attenuation of sound speed depends mostly on the SST change in the upper layers of the ocean. In this section we assess the impact of this variability on the local EM and acoustic propagation characteristics.

The surface evaporation duct height (EDH) is a measure of how far the radar beam travels before fallout. The radar detection range is an increasing function of the surface EDH. Pappert and Paulus (1992) estimated that the ranges in standard atmospheric conditions are about

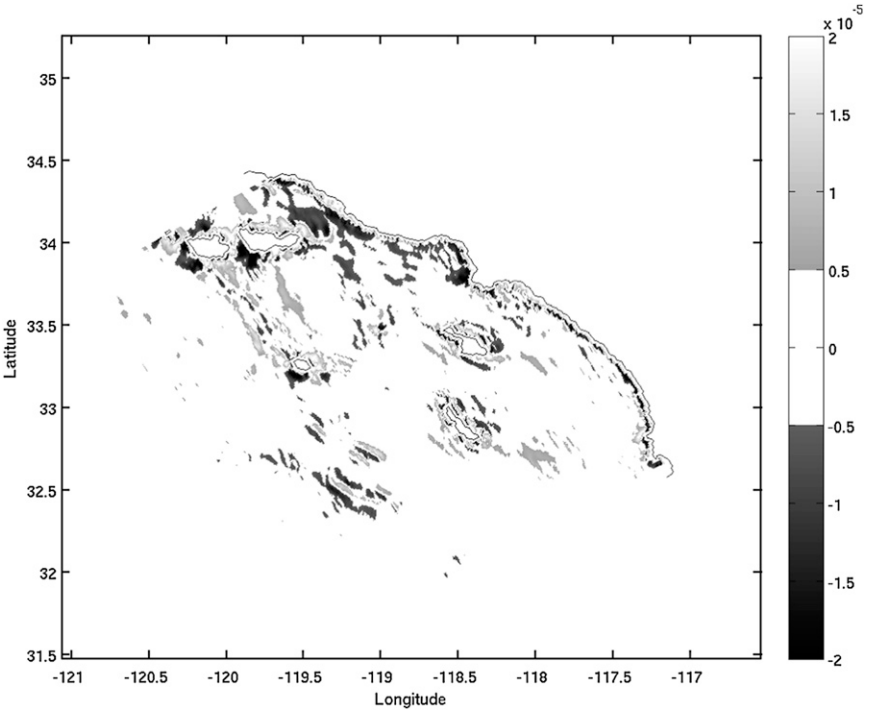

FIG. 22. The current vorticity ($\times 10^{-5}$ s^{-1}) from ocean grid 2. The current-induced wakes are represented by the narrow strips of negative (darker shade) and positive (lighter shade) vorticity values.

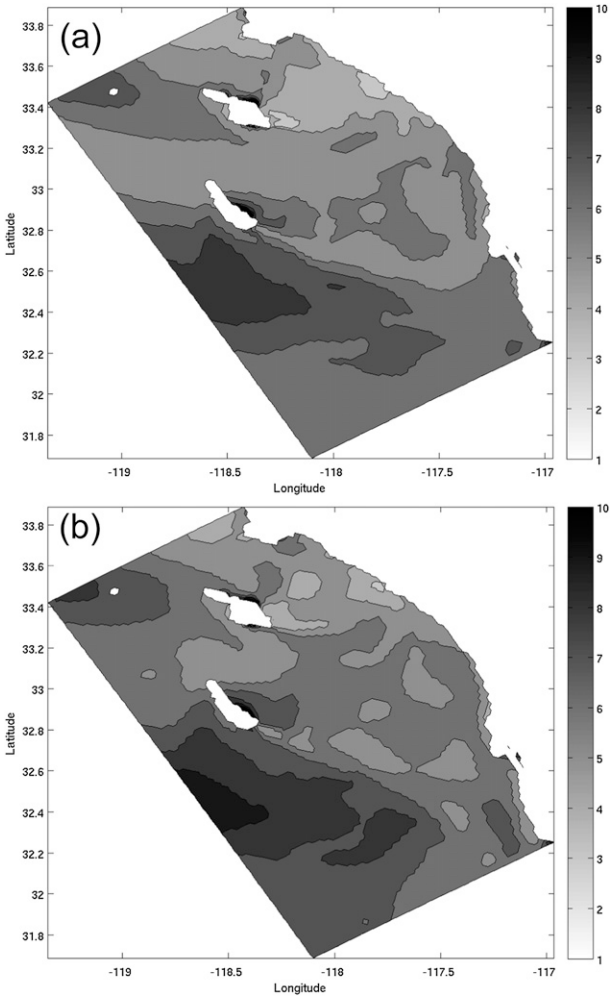

FIG. 23. Model-simulated EDH (m) at 24 h from the (a) coupled and (b) uncoupled runs. The uncoupled run has an average EDH 1 m s^{-1} higher than the coupled run.

35 km for the 0-m duct, 61 km for the 14-m duct, and 81 km for the 28-m duct. In COAMPS, the EDH is computed as the height of the minimum of the modified refractivity profile (*M* profile). The *M* profile is obtained based on Monin–Obukhov similarity theory, which is a function of the SST, air temperature, relative humidity, and wind speed (Burk et al. 2003). The surface ducting condition occurs when there is a rapid decrease of humidity with height above the sea surface. The surface EDH pattern from the coupled and uncoupled runs is similar. The EDH is approximately 6 m in the San Clemente and 3 m in the Santa Catalina wake zones (Fig. 23). The coupled run, on average, has an approximately 1-m lower EDH than the uncoupled run. The EDH difference is small. However, the surface EDH pattern from the coupled run is more uniform, which is due to the general, cold, wintertime upwelling SST feedback to the lower atmospheric layer in the Southern California Bight region.

In the ocean, the refraction of sound speed depends on the 4D (temporal and spatial) variation of the governing factors of pressure, ocean temperature, and salinity. Sound speed is affected primarily by the temperature change in the upper ocean. The island wakes in the Southern California Bight create SST variations in the ocean mixed layer, which, in turn, generate fluctuations of the sound speed within 50 km of the wake zone in the top 20 m of the ocean as shown in Fig. 24. This kind of variability can cause the horizontal refraction of sound speed bias in the cross-ray direction (Godin et al. 2006).

4. Summary

We have shown the air–ocean coupling effect in high- and low-wind regimes using the ESMF coupling technology. The coupled system is tested in two cases. In the first case study of Hurricane Katrina, the coupled model is able to reduce the TC intensity through the negative feedback of the cold wake response from the ocean. It is shown that, within the ocean mixed layer, both horizontal and vertical advection can be as important as the wind-induced vertical mixing in increasing the width and magnitude of the wake. The production of the TC cold wake not only reduces the net heat and moisture fluxes from the ocean to the storm but also increases the asymmetry of the TC thermodynamic and dynamic structure. In the case investigated here, these changes lead to a maximum increase of the eye size of 10 km and a 10% decrease of the hurricane-force wind radius. The atmospheric response to the cold wake produces an increase in convergence in the TC northeast and northwest quadrants and a decrease in convection in the southwest quadrant. Similar to the observations, the coupled run develops an open-eye structure 2 h prior to landfall, while the uncoupled run still has a closed eye. The opening of the eye in the coupled run is associated with the dry inner-core downdraft below 3-km height in the southwest quadrant. The wind asymmetry in the dry, idealized, axisymmetric vortex simulation indicates that the cold wake induces a wavenumber 3 response. The wake also forces an area of downward motion upwind from the wake and an area of upward motion on top of the wake. When the wake is reduced to half of its original width, the magnitude and size of the induced waves are decreased.

In the second case study, we used the coupled model to examine the wind-induced and current-induced island wakes in the Southern California Bight and the impact of these wakes on EM and acoustic propagation. In the 1.67-km atmospheric domain, long, straight wind wakes that extend longer than the length of the islands are

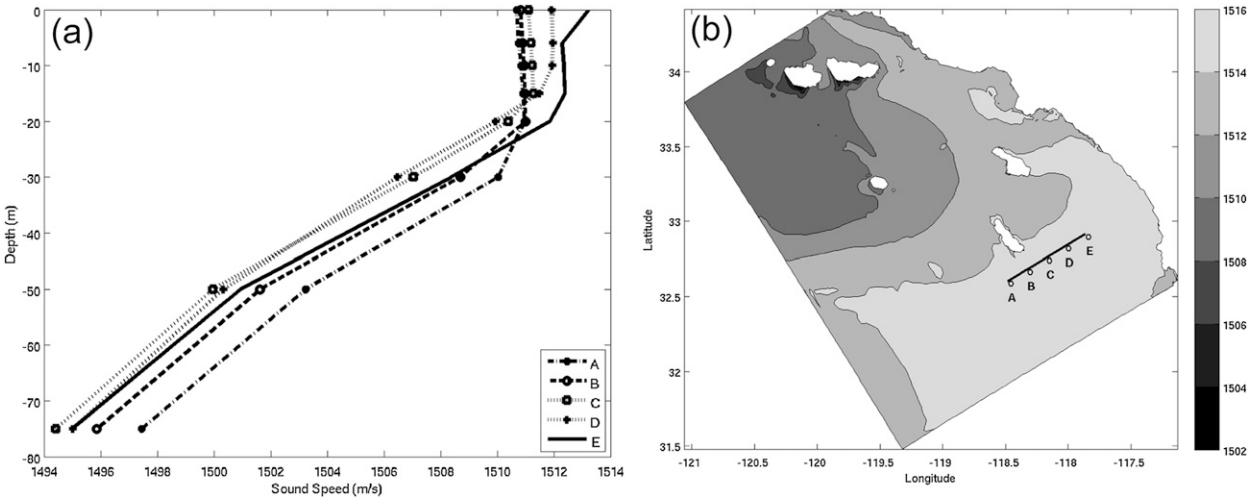

FIG. 24. (a) Model-simulated upper-ocean sound speed (m s^{-1}) profiles taken in the wake region of San Clemente Island and (b) ocean-surface sound-speed distribution.

produced south of Santa Catalina and San Clemente islands. These wind wakes are caused by mountain wave breaking from the island topography that peaks near 600 m. Accompanying these conditions is a minimum in the wind stress and negative stress curl. The current-induced wakes occur south of all the Channel Islands. The coupled model is able to produce pairs of counter-rotating eddies with a horizontal scale of 10–15 km.

There are still many important coupling issues that are not covered by the present study, including the coupled model validation and the effect of coupling frequency. Running the high-resolution coupled model presents new challenges for validation because of the need for high-resolution, collocated observations in both the ocean and atmosphere. The immediate extension of the coupled system described here is the inclusion of a wave-model component in a three-way coupled mode to explicitly account for the wave-induced stress feedback to the ocean current and to the atmospheric low-level wind.

Acknowledgments. The authors thank Dr. Paul May of SAIC for providing the software to generate the NCOM initial and boundary conditions for our second test case. We also appreciate discussions with Dr. Michael Montgomery of NPS regarding the TC vortex dynamics. We thank Drs. Jerome Schmidt and Peter Black of NRL Monterey and anonymous reviewers for their insightful suggestions on the revision of the manuscript. We would like to acknowledge Ms. Cecelia DeLuca and Mr. Gehard Theurich of the National Center for Atmospheric Research for the ESMF software upgrade and technical support. The funding that supported the completion of this project is provided by the Department of Defense High Performance Computer Modernization Program.

APPENDIX

The ESMF Coupling Tool

The ESMF system is used in two tiers within COAMPS. On the top level, the ESMF superstructure is used to advance the coupled system forward in time. On the lower level, the ESMF regrid infrastructure is used to communicate intracomponent grid information across any number of processors.

The basic method used to interpolate arrays from one ESMF component to another is the sparse-matrix multiplication method. Although a direct mapping of data from any given component (e.g., the atmosphere) to any other component (e.g., the ocean) is possible, it turns out that the process to compute the weights used to interpolate a set number of points from one component to a fixed point in the other is a rather complicated bookkeeping process on a parallel computing platform. To simplify the problem, we break down the process into two basic steps. The first step is to create an independent exchange grid for each component used in the coupling. The second step is to interpolate between each pair of exchange grids. Conceptually, either exchange grid can be composed of a uniform (structured) or nonuniform grid; however, since the atmospheric nests may move during a given forecast, the structured exchange grid approach is simpler in practice.

The purpose of the exchange grids is to allow one to first merge data derived from multiple nests of either

component onto a single contiguous grid prior to the interpolation step.

After merging, the data on each exchange grid are now ready for regridding to the appropriate component requesting the data. By regridding we are referring to the process where data on any given source exchange grid is interpolated onto the target exchange grid. The source grid point weights on the exchange grids that are used to interpolate to the destination points of the receiving component are computed only once after the configuration of the exchange grids is determined.

The coupler component

The main purpose of the coupler component is to perform an interpolation of the fields on the exchange grid between each pair of coupled components. We used the ESMF regrid infrastructure, mainly the sparse matrix multiply API, to do the regridding. We developed our own algorithm to create the regrid weights. The weights for regridding are computed internally in the coupler to take care of differences that may arise between exchange grids, such as the map projections and land–sea tables. In addition, because the land and sea points have different characteristics, values at the atmospheric grid points that are over land should not be used when interpolating fields such as wind stress to a given ocean only point. Therefore, an algorithm that uses the nearest neighbor or a second-order Taylor series extrapolation is added to provide the total transformation values as shown by the following equation:

$$g_j = \sum_{i=1}^{N_S} f_i \left(\sum_{k=1}^{N_S} \mathbf{C}_{ik} \mathbf{R}_{kj} \right) = \sum_{i=1}^{N_S} f_i \mathbf{T}_{ij}.$$

In this expression g_j is the destination grid value, j is the destination grid index, f_i is the source grid value, i is the source grid index, $\mathbf{C}_{ik}$ is a $i \times k$ matrix that holds the weights for the extrapolation, k is the size of the source grid, $\mathbf{R}_{kj}$ is a $k \times j$ matrix that holds the weights for the interpolation, and $\mathbf{T}_{ij}$ is the total transformation matrix used for regridding. Since only source points that are close to the destination points have a nonzero weight, the $\mathbf{C}$ and $\mathbf{R}$ matrices are sparse. These matrices are recast to one-dimensional arrays for computational efficiency. The final step that the coupler performs is to merge the global NCOM SST from the ocean background component onto the atmospheric exchange grid during the ocean export phase. This step provides the SST updates for atmospheric grid points that lie outside the ocean coarse domain. The SST update is either specified using the operational global NCOM forecast (gNCOM), held constant in time using the NCODA analysis, or simply set to a single constant value.

REFERENCES

Andreas, E. L, and K. A. Emanuel, 2001: Effects of sea spray on tropical cyclone intensity. *J. Atmos. Sci.,* **58,** 3741–3751.

Bao, J.-W., J. M. Wilczak, J.-K. Choi, and L. H. Kantha, 2000: Numerical simulations of air–sea interaction under high wind conditions using a coupled model: A study of hurricane development. *Mon. Wea. Rev.,* **128,** 2190–2210.

Bender, M. A., and I. Ginis, 2000: Real-case simulations of hurricane–ocean interaction using a high-resolution coupled model: Effects on hurricane intensity. *Mon. Wea. Rev.,* **128,** 917–946.

——, ——, R. Tuleya, B. Thomas, and T. Marchok, 2007: The operational GFDL coupled hurricane–ocean prediction system and a summary of its performance. *Mon. Wea. Rev.,* **135,** 3965–3989.

Black, P. G., and Coauthors, 2007: Air–sea exchange in hurricanes: Synthesis of observations from the coupled boundary layer air–sea transfer experiment. *Bull. Amer. Meteor. Soc.,* **88,** 357–374.

Burk, S. D., T. Haack, L. T. Rogers, and L. J. Wagner, 2003: Island wake dynamics and wake influence on the evaporation duct and radar propagation. *J. Appl. Meteor.,* **42,** 349–367.

Caldeira, R. M. A., P. Marchesiello, N. P. Nezlin, P. M. DiGiacomo, and J. C. McWilliams, 2005: Island wakes in the Southern California Bight. *J. Geophys. Res.,* **110,** C11012, doi:10.1029/2004JC002675.

Chen, S., and Coauthors, 2003: COAMPS version 3 model description. NRL Rep. NRL/PU/7500-04-448, 143 pp.

Chen, S. S., J. F. Price, W. Zhao, M. A. Donelan, and E. D. Walsh, 2007: The CBLAST-Hurricane Program and the next generation fully coupled atmosphere–wave–ocean models for hurricane research and prediction. *Bull. Amer. Meteor. Soc.,* **88,** 311–317.

Davis, C., and Coauthors, 2008: Prediction of landfalling hurricanes with the advanced hurricane WRF model. *Mon. Wea. Rev.,* **136,** 1990–2005.

Didlake, A. C., Jr., and R. A. Houze Jr., 2009: Convective-scale downdrafts in the principal rainband of Hurricane Katrina (2005). *Mon. Wea. Rev.,* **137,** 3269–3293.

DiGiacomo, P., and B. Holt, 2001: Satellite observations of small coastal ocean eddies in the Southern California Bight. *J. Geophys. Res.,* **106,** 22 521–22 543.

Donelan, M. A., B. K. Haus, N. Reul, W. J. Plant, M. Stiassnie, H. C. Graber, O. B. Brown, and E. S. Saltzman, 2004: On the limiting aerodynamic roughness of the ocean in very strong winds. *Geophys. Res. Lett.,* **31,** L18306, doi:10.1029/2004GL019460.

Dong, C., and J. C. McWilliams, 2007: A numerical study of island wakes in the Southern California Bight. *Cont. Shelf Res.,* **27,** 1233–1248.

Fairall, C., E. Bradley, J. Hare, A. Grachev, and J. Edson, 2003: Bulk parameterization of air–sea fluxes: Updates and verification for the COARE algorithm. *J. Climate,* **16,** 571–591.

Godin, O. A., V. U. Zavorotny, A. G. Voronovich, and V. V. Goncharov, 2006: Refraction of sound in a horizontally inhomogeneous, time-dependent ocean. *J. Ocean Eng.,* **31,** 384–401.

Hence, D. A., and R. A. Houze Jr., 2008: Kinematic structure of convective-scale elements in the rainbands of Hurricanes Katrina and Rita (2005). *J. Geophys. Res.,* **113,** D15108, doi:10.1029/2007JD009429.

Hodur, R. H., 1997: The Naval Research Laboratory's Coupled Ocean–Atmosphere Mesoscale Prediction System (COAMPS). *Mon. Wea. Rev.,* **125,** 1414–1430.

Hong, X., S. W. Chang, S. Raman, L. K. Shay, and R. H. Hodur, 2000: The interaction between Hurricane Opal (1995) and a warm core ring in the Gulf of Mexico. *Mon. Wea. Rev.,* **128,** 1347–1365.

Jin, Y., W. Thompson, S. Wang, and C. Liou, 2007: A numerical study of the effect of dissipative heating on tropical cyclone intensity. *Wea. Forecasting,* **22,** 950–965.

Louis, J.-F., 1979: A parametric model of vertical eddy fluxes in the atmosphere. *Bound.-Layer Meteor.,* **17,** 187–202.

Martin, P. J., 2000: Description of the NAVY coastal ocean model version 1.0. NRL Rep. NRL/FR/7322-00-9962, 42 pp.

——, J. W. Book, and J. D. Doyle, 2006: Simulation of the northern Adriatic circulation during winter 2003. *J. Geophys. Res.,* **111,** C03S12, doi:10.1029/2006JC003511.

Pappert, R. A., and R. A. Paulus, 1992: Sea echo in tropospheric ducting environments. *Radio Sci.,* **27,** 189–209.

Prasad, T. G., and P. J. Hogan, 2007: Upper-ocean response to Hurricane Ivan in a 1/25° nested Gulf of Mexico HYCOM. *J. Geophys. Res.,* **112,** C04013, doi:10.1029/2006JC003695.

Price, J. F., 1981: Upper ocean response to a hurricane. *J. Phys. Oceanogr.,* **11,** 153–175.

——, T. B. Sanford, and G. Z. Forristall, 1994: Forced stage response to a moving hurricane. *J. Phys. Oceanogr.,* **24,** 233–260.

——, J. Morzel, and P. Niiler, 2008: Warming of SST in the cool wake of a moving hurricane. *J. Geophys. Res.,* **113,** C07010, doi:10.1029/2007JC004393.

Pullen, J., J. D. Doyle, R. H. Hodur, A. Ogston, J. W. Book, H. Perkins, and R. P. Signell, 2003: Coupled ocean-atmosphere nested modeling of the Adriatic Sea during winter and spring 2001. *J. Geophys. Res.,* **108,** 3320, doi:10.1029/2003JC001780.

Small, R. J., and Coauthors, 2008: Air-sea interaction over ocean fronts and eddies. *Dyn. Atmos. Oceans,* **45,** 274–319.

Spall, M. A., 2007: Midlatitude wind stress–sea surface temperature coupling in the vicinity of oceanic fronts. *J. Climate,* **20,** 3785–3801.

Zhu, H., U. Wolfgang, and S. K. Roger, 2004: Ocean effects on tropical cyclone intensification and inner-core asymmetries. *J. Atmos. Sci.,* **61,** 1245–1258.